

A large deformation theory for coupled swelling and growth with application to growing tumors and bacterial biofilms

S. Chockalingam^a, T. Cohen^{b,c,*}

^a*Massachusetts Institute of Technology, Department of Aeronautics and Astronautics, Cambridge, MA, 02139, USA*

^b*Massachusetts Institute of Technology, Department of Civil and Environmental Engineering, Cambridge, MA, 02139, USA*

^c*Massachusetts Institute of Technology, Department of Mechanical Engineering, Cambridge, MA, 02139, USA*

Abstract

There is significant interest in modelling the mechanics and physics of growth of soft biological systems such as tumors and bacterial biofilms. Solid tumors account for more than 85% of cancer mortality and bacterial biofilms account for a significant part of all human microbial infections. These growing biological systems are a mixture of fluid and solid components and increase their mass by intake of diffusing species such as fluids and nutrients (swelling) and subsequent conversion of some of the diffusing species into solid material (growth). Experiments indicate that these systems swell by large amounts and that the swelling and growth are intrinsically coupled, with the swelling being an important driver of growth. However, many existing theories for swelling coupled growth employ linear poroelasticity, which is limited to small swelling deformations, and employ phenomenological prescriptions for the dependence of growth rate on concentration of diffusing species and the stress-state in the system. In particular, the termination of growth is enforced through the prescription of a critical concentration of diffusing species and a homeostatic stress. In contrast, by developing a fully coupled swelling-growth theory that accounts for large swelling through nonlinear poroelasticity, we show that the emergent driving stress for growth automatically captures all the above phenomena. Further, we show that for the soft growing systems considered here, the effects of the homeostatic stress and critical concentration can be encapsulated under a single notion of a critical swelling ratio. The applicability of the theory is shown by its ability to capture experimental observations of growing tumors and biofilms under various mechanical and diffusion-consumption constraints. Additionally, compared to generalized mixture theories, our theory is amenable to relatively easy numerical implementation with a minimal physically motivated parameter space.

Keywords: Swelling, Nonlinear poroelasticity, Growth, Tumor growth, Bacterial biofilms, Homeostatic stress

1. Introduction

Understanding the mechanics and physics of growth of soft biological systems ranging from cellular systems such as tumors and bacterial biofilms to tissues and organs such as arteries,

*Corresponding author: talco@mit.edu

lungs, skin, and the brain (Araujo and McElwain, 2004; Kuhl, 2014; Jain et al., 2014; Mattei et al., 2018), can aid in development of clinical therapies and diagnosis that have important societal implications. For example, solid tumors account for more than 85% of cancer mortality (Jain, 2005). Similarly, bacterial biofilms, aggregates of bacterial cells held together by an extracellular matrix, account for a significant part of all human microbial infections (Bryers, 2008). These growing biological systems are a mixture of solid components such as cells and extracellular matrix, and diffusing fluid components with dissolved solutes such as nutrients, oxygen, and growth factors. They increase their mass by intake of diffusing species from their surroundings, the process of swelling, and subsequent conversion of some of the diffusing species into additional solid material, a process henceforth referred to here as growth.

Experiments on bacterial biofilms indicate that swelling and growth are intrinsically coupled and that swelling is an important driver of growth (Seminara et al., 2012; Yan et al., 2017). The diffusing fluids supply the mass for growth and dissolved species such as nutrients, oxygen and growth factors significantly affect the growth rate. In particular, the growth rate typically increases with the concentration of diffusing species, saturating at high concentrations (Monod, 1949; Casciari et al., 1992; Narayanan et al., 2010) while the growth rate at small concentrations is well captured using a critical concentration below which growth is assumed to stop (Greenspan, 1972; Hlatky et al., 1988; Ward and King, 1997; Bertuzzi et al., 2010; Araujo and McElwain, 2004; Xue et al., 2016). There are other considerations which also make it important to account for swelling during the growth process. For example, it is known that cell packing density of tumor cells (which is inversely related with the amount of swelling) increases when they grow against a stiff medium (Helmlinger et al., 1997) or through application of external pressure (Koike et al., 2002; Alessandri et al., 2013; Chalut and Janmey, 2014) and such compaction can set the basis for a multicellular-dependent mechanism of increased radiation resistance and both intrinsic and acquired drug resistance (Olive and Durand, 1994; Kobayashi et al., 1993; Kerbel et al., 1994; Croix et al., 1996). Similarly, compactness of bacterial biofilms, which also increases with confining stiffness (SI of Zhang et al. (2021)), is a key determinant of underlying resistance to invader cells (Nadell et al., 2015; Yan et al., 2017). A fundamental understanding of the physics of coupled swelling-growth in these systems can aid potential development of clinical therapies, for example, Croix et al. (1996) showed that a decrease in cell compaction, as induced by hyaluronidase treatment of tumor spheroids, alleviated multicellular-dependent drug resistance. Similarly, Yan et al. (2017) demonstrate the possibility of using external osmolytes to control the compactness of pathogenic biofilms, which is critical to the penetration of antibiotic molecules.

Further, the extracellular matrix in these cellular systems are akin to hydrogels and can swell by significant amounts (Yan et al., 2017) where the solid volume fraction can be as low as 20% (SI of Zhang et al. (2021) and Section 5.7 of this manuscript). Thus a large deformation coupled swelling-growth theory is required to accurately characterize and elucidate the physics in these growing systems. However, current growth theories that account for diffusing species typically either model the diffusion as an auxiliary process that neglects swelling, mechanics coupling, and mass balance (Ambrosi and Mollica, 2002, 2004; Ambrosi and Guillou, 2007; Kim et al., 2011; Ciarletta et al., 2013), or employ linear poroelasticity (Roose et al., 2003; Sarntinoranont et al., 2003; Xue et al., 2016; Sacco et al., 2017; Xue et al., 2018; Carpio et al., 2019) based on the seminal works of Biot (Biot, 1941; Biot and Temple, 1972), which is limited to relatively small

deformations (Bouklas and Huang, 2012). Mixture theories of growth on the other hand account for the mechanics and motion of every phase in the growing body (Humphrey and Rajagopal, 2002; Ambrosi and Preziosi, 2002; Byrne et al., 2003; Garikipati et al., 2004; Ateshian, 2007; Azeloglu et al., 2008; Narayanan et al., 2009; Ateshian and Ricken, 2010; Chatelain et al., 2011; Ciarletta et al., 2011; Amar et al., 2011; Ateshian et al., 2012, 2014; Myers and Ateshian, 2014; Faghihi et al., 2020) and can account for large deformations and the coupling between swelling and growth. However they also suffer from several drawbacks - (i) The requirement for specification of a large number of constitutive relations and associated material parameters (Ambrosi et al., 2011; Oden et al., 2016) that can be both impractical to experimentally determine and to model, (ii) Difficulties associated with specifying boundary conditions and in dealing with partial stresses and mass exchanges between the single phases (Ambrosi et al., 2010), and (iii) Complexity of numerical implementation with more equations being modelled than might be necessary to describe the required physics.

In addition to the shortcomings discussed above, a major limitation of the vast majority of growth theories in the literature is the use of phenomenological prescriptions to capture important experimental observations. For example, most growth theories capture the earlier discussed dependence of the growth rate on concentration of diffusing species using phenomenological prescriptions including a critical concentration that halts growth. Similarly, when it comes to the effects of mechanical constraints, it is generally known that applied compressive stresses deter volumetric growth. A widely established concept in the literature is that of ‘homeostatic stress’, which prescribes a preferred stress state that growing systems tend towards and upon reaching which the growth process halts (Rodriguez et al., 1994; Taber, 1998; Fung, 2013). In terms of theory development, the homeostatic stress is mostly introduced in an ad hoc phenomenological fashion (Rodriguez et al., 1994; Taber, 1998; DiCarlo and Quiligotti, 2002; Lubarda and Hoger, 2002; Ambrosi and Guana, 2007; Menzel and Kuhl, 2012; Mpekris et al., 2015; Xue et al., 2016; Curatolo et al., 2017). Under compressive stress states, which is generally the case for many of these growing systems, this ad hoc homeostatic term often becomes the primary positive driving term in evolution laws for the growth process. This kinematic modelling of the physics does not explain the kinetic origins of these phenomena starting from the underlying mechanisms. It further limits the confidence in general applicability of the theories to scenarios beyond the specific experimental data they are calibrated to capture.

In light of all the above considerations, the goal of this manuscript is *to formulate a homogenized single phase continuum theory for fully coupled swelling and growth that accounts for large swelling deformations and mass balance, while capturing important coupled swelling-growth phenomena using underlying kinetics instead of ad hoc kinematic prescriptions.* To do so, we will augment growth modelling frameworks (Rodriguez et al., 1994; DiCarlo and Quiligotti, 2002; Ambrosi and Mollica, 2002; Ambrosi and Guillou, 2007; Ambrosi and Guana, 2007; Menzel and Kuhl, 2012; Kuhl, 2014) with nonlinear poroelasticity formulations developed for soft swelling elastomers and polymeric gels (Hong et al., 2008; Doi, 2009; Duda et al., 2010; Chester and Anand, 2010, 2011; Lucantonio et al., 2013; Liu et al., 2015) and prescribe the swelling and growth evolution using the kinetic driving terms that arise naturally. We note in passing that a nonlinear poroelastic swelling growth model has also been developed in Fraldi and Carotenuto (2018), assuming moderate variations in fluid content. A large deformation swelling-growth the-

ory has also been developed by Curatolo et al. (2017), in the context of bulking of wood, wherein growth is simply a change in relaxed state instead of an increase in mass of the solid as considered here, while employing phenomenological prescriptions including for the homeostatic stress. See also Dervaux and Amar (2011) where instability arising from large deformation growth is compared with that arising from large swelling.

The paper is organized as follows. In Section 2, we begin by discussing a set of tumor growth experiments that encapsulate all the phenomena discussed above and use it to motivate the theory development and analysis to follow in subsequent sections. The governing equations of the theory are then developed in Section 3. The theory is specialized in Section 4 by choosing specific forms of the constitutive functions and non-dimensionalized to allow for ease of analysis and to make limiting approximations. Subsequently, in Section 5 we analyze the theory and use it to solve boundary value problems and model experiments of growing tumor and bacterial biofilms. We provide some concluding remarks in Section 6.

2. Motivating example of tumor growth experiments

To motivate the theory development in the following sections, we begin by discussing a set of tumor growth experiments that encapsulates the complete spectrum of phenomena that the theory should capture.

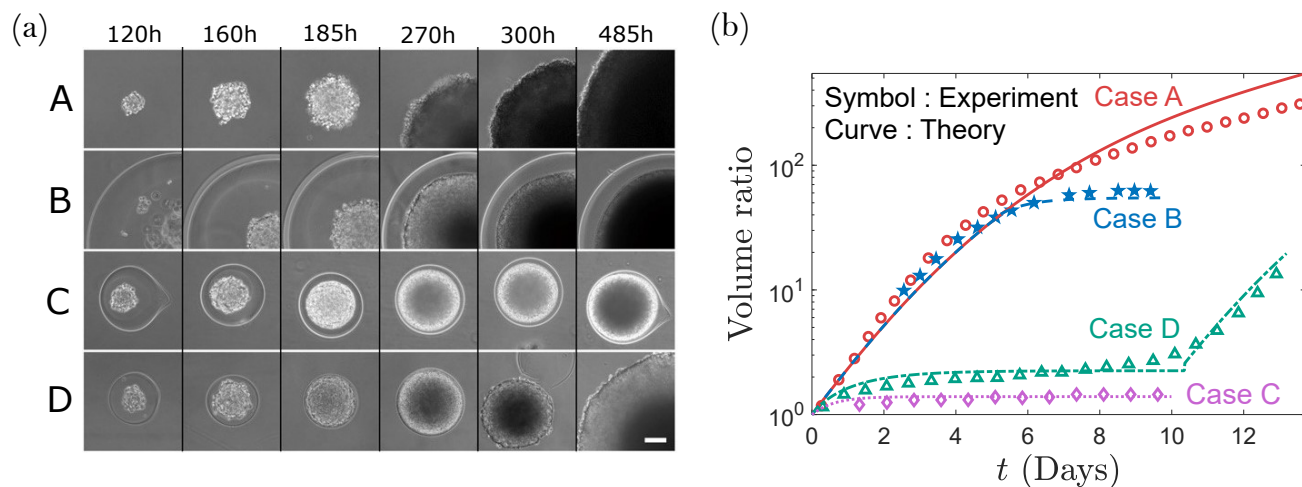


Figure 1: (a) Experiments of *in vitro* spheroid tumor growth in four different environments: (A) free growth, (B) large and thick microcapsule confinement, (C) small and thick microcapsule confinement, and (D) small and thin microcapsule confinement that breaks. Scale bar: 50 μm . Reprinted from Alessandri et al. (2013). (b) Comparison of experimental data of time evolution of tumor volume ratio (ratio of tumor volume at time t to its value at $t = 0$) with predictions of our swelling growth theory (see Section 5.6). Volume of tumor at $t = 0$ is 0.003 mm^3 .

Alessandri et al. (2013) performed microfluidic experiments to study tumor growth in response to mechanical confinement using spheroids of CT26 mouse colon carcinoma cells. The experiments studied multiple scenarios: free growth with no confinement (Case A) and growth under the confinement of alginate microcapsules of different radii and thicknesses (Cases B - D). Images from the experiments are shown in Figure 1(a) while the experimental data for the

evolution of the tumor volume ratio (ratio of volume at time t to its value at $t = 0$) is plotted in Figure 1(b). The experimental data was time-shifted so that in all cases, the volume at $t = 0$ is 0.003 mm^3 which is the inner volume of the smallest confining microcapsule. The microcapsules were permeable and thus the surface of the tumors were supplied with required fluids, nutrients and oxygen for growth. Below are the observations for these four typically studied cases.

1. In Case A, the free growth is initially exponential followed by a power-law volume increase. Further growth leads to a necrotic/dying core while growth is confined to thin rim of proliferating cells.
2. In Case B, the tumor undergoes free growth until it comes in contact with a large and thick microcapsule following which the growth rate is rapidly suppressed.
3. In Case C, the tumor is confined by a small and thick microcapsule, and the growth is inhibited by the confinement as it deforms.
4. In Case D, the tumor is confined by a small and thin microcapsule. The growth rate falls as the tumor expands against the confinement but the large deformation causes the microcapsule to burst following which the tumor resumes exponential growth similar to free-growth case.

Conventional growth theories would capture these experiments using phenomenological prescriptions for the established phenomena discussed in Section 1, namely the growth rate dependence on concentration of diffusing species and applied stresses, and in particular the existence of a critical concentration and homeostatic stress (Xue et al., 2016). The diffusion of fluids and dissolved nutrients from the outside of the tumor to its core, combined with consumption for growth leads to a radially decreasing concentration profile from the outside to inside. While the outer edge of the growing body remains replenished with diffusing species, the spatial decrease of concentration towards the core becomes more pronounced as the body grows exponentially to larger sizes. Initially the concentration everywhere is high and the growth rate is at a saturated value leading to the exponential growth. But at larger sizes the growth rates are spatially decreasing towards the core leading to the decrease in overall growth rate. The growth in the core halts when the concentration reaches the critical value. Eventually most of the tumor stops growing and the growth localizes to a very thin proliferating ring near the outside. Further, increasing compressive stresses when growing against mechanical confinement causes the growth rate to fall off, till the homeostatic value is reached when growth halts and a steady size is reached. In the case of thin confinement, the confinement breaks before homeostatic stress is reached, leading to resumption of free-growth.

Such modelling of the above experiments is fundamentally handicapped by the reliance on phenomenological prescriptions and raises several questions. Why does the growth process accelerate with increasing concentration of diffusing species while saturating at high values and what causes it to halt below a critical concentration? Why is there a mechanical stress state that halts growth? Can these seemingly unlinked diffusion-consumption and mechanical phenomena be described by a unified kinetic theory? We will answer these questions in the following sections by developing a fully coupled large deformation swelling-growth theory where we use the kinetic driving stress that naturally arises to model the growth process.

3. Theory

The key ingredients and assumptions of the swelling-growth theory are summarized below following which we develop the theory.

1. Solid components such as cells and the extracellular matrix are abstracted and their behavior is assumed to be described by models for hydrogels.
2. While biological growth generally depends on several diffusing components such as water/fluids, nutrients, oxygen, glucose, and growth factors, we consider a single representative fluid phase whose concentration reflects the concentration of dissolved solutes, which we henceforth refer to as the diffusing species. Though the physical or mechanical swelling is primarily a result of the diffusing water, the bio-chemical energy of the dissolved components such as nutrients and growth factors is an important driver of growth. While the theory here can be generalized to multiple diffusing components, we will show that a single representative species is sufficient to capture the essential physics.
3. The consumption of the diffusing species supplies the mass for solid growth. The remaining diffusing species swells the grown solid. While growth can involve various complex cellular processes including cell division and production of extracellular matrix, considering continuum scale phenomena here, it is abstracted as conversion of the diffusing species into additional solid material. The chemical energy for the conversion process is thus a homogenized value from all the underlying cellular processes.
4. The growing body is described by a fixed set of material points and growth and swelling are modelled as an increase in volume of these material points in appropriate relaxed spaces mapped from a reference space through the widely employed decomposition of deformation gradient (Rodriguez et al., 1994; Ambrosi and Mollica, 2002; Chester and Anand, 2010). The volume increases correspond to an increase in mass of the homogenized continuum through closure of mass balance. This is in contrast to several growth theories in the literature where an intrinsic mass supply is assumed and open system thermodynamics is employed (Ambrosi and Mollica, 2004; Kuhl, 2014; Xue et al., 2016).
5. We neglect any viscoelastic and inertial effects at the timescale of growth.

3.1. Kinematics

Consider an initial compatible dry reference configuration of the body in the absence of diffusing species denoted by \mathcal{B}^R . Let \mathcal{B}^t denote the current/observed configuration of the swelling and growing body at time t . Consider a material point at the position \mathbf{X} in the dry reference configuration whose position in the current configuration is given by $\mathbf{x} = \varphi(\mathbf{X}, t)$. We define the deformation gradient \mathbf{F} and its decomposition as follows¹ (see Figure 2)

$$\mathbf{F} = \nabla\varphi = \mathbf{F}^{es}\mathbf{F}^g = \mathbf{F}^e\mathbf{F}^s\mathbf{F}^g, \quad \mathbf{F}^s = \lambda^s \mathbf{I}, \quad \mathbf{F}^{es} = \mathbf{F}^e\mathbf{F}^s \quad (1)$$

where \mathbf{F}^g is the growth tensor describing the change in solid mass, \mathbf{F}^s is the swelling tensor describing the change in mass due to diffusing species, and \mathbf{F}^e is the elastic deformation tensor. The swelling tensor is taken to be isotropic where λ^s is the swelling stretch (similar to Chester

¹The Lagrangian spatial gradient operator $\nabla(\cdot)$ is defined as $\nabla(\cdot) = \frac{\partial(\cdot)}{\partial\mathbf{X}}$

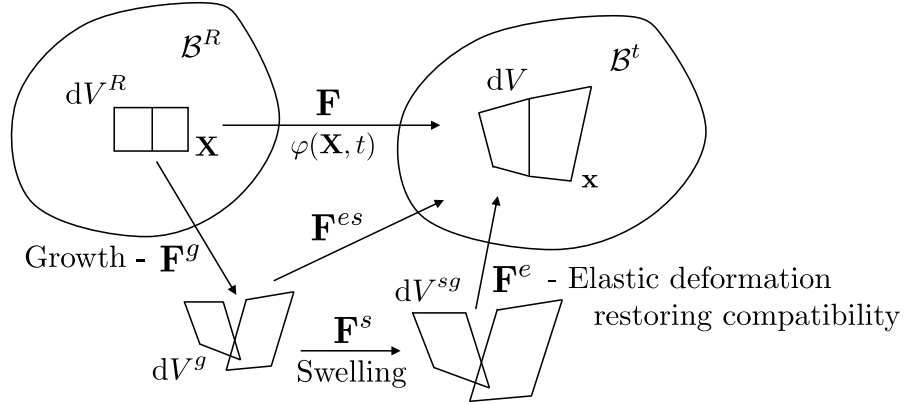


Figure 2: Decomposition of the deformation gradient.

and Anand (2010, 2011)). The growth tensor \mathbf{F}^g maps the material point at \mathbf{X} in the dry reference configuration to its relaxed unswollen state that would be obtained if the particle associated with \mathbf{X} is cut out from the body and drained of its diffusing species content while retaining the mass of the solid skeleton. The density of the solid matrix is assumed to be constant from its value in dry reference space, ρ_0^m , through the mapping by \mathbf{F}^g . The tensor $\mathbf{F}^{es}(\mathbf{X})$ maps the relaxed unswollen state to the current state of the particle. Note that the configuration of the body in the intermediate spaces mapped by \mathbf{F}^g and \mathbf{F}^s do not have any physical requirement of compatibility unlike \mathcal{B}^t . The displacement \mathbf{u} is defined as $\mathbf{u}(\mathbf{X}, t) = \mathbf{x} - \mathbf{X}$.

We define the following volumetric ratios (all assumed to be positive)

$$J^g = \det \mathbf{F}^g, \quad J^s = \det \mathbf{F}^s = (\lambda^s)^3, \quad J^e = \det \mathbf{F}^e, \quad (2)$$

$$J^{es} = \det \mathbf{F}^{es} = J^e J^s, \quad J = \det \mathbf{F} = J^g J^e J^s, \quad (3)$$

such that the volume of a particle in the dry reference space, dV^R , relates to its current volume dV and volume in the intermediate grown and swollen-grown spaces, dV^g and dV^{sg} respectively, as

$$dV^g = J^g dV^R, \quad dV^{sg} = J^s J^g dV^R, \quad dV = J dV^R \quad (4)$$

The volume fraction of solid, ϕ , is then defined as

$$\phi = \frac{dV^g}{dV^{gs}} = \frac{J^g dV_R}{J^g J^s dV_R} = \frac{1}{J^s} \quad (5)$$

so that it is inversely related to the swelling ratio J^s . We have the physical requirement $\phi \in (0, 1]$ or equivalently $1 \leq J^s < \infty$. Let dA and dA_R denote corresponding area elements in the current and dry reference space with outward pointing normals \mathbf{n} and \mathbf{n}_R , respectively. They are related by Nanson's formula - $\mathbf{n} dA = J \mathbf{F}^{-T} \mathbf{n}_R dA_R$.

The following deformation tensors are defined for later use,

$$\mathbf{C}^e = \mathbf{F}^{eT} \mathbf{F}^e, \quad \mathbf{C}^{es} = \mathbf{F}^{esT} \mathbf{F}^{es} = (J^s)^{\frac{2}{3}} \mathbf{C}^e, \quad \mathbf{B}^e = \mathbf{F}^e \mathbf{F}^{eT}, \quad \mathbf{B}^{es} = \mathbf{F}^{es} \mathbf{F}^{esT} = (J^s)^{\frac{2}{3}} \mathbf{B}^e \quad (6)$$

Using eq. (1), we can derive the following rate relation

$$\mathbf{L} = \dot{\mathbf{F}}\mathbf{F}^{-1} = \mathbf{L}^e + \mathbf{F}^e\mathbf{L}^g\mathbf{F}^{e-1} + \frac{\dot{J}^s}{3J^s}\mathbf{I} \quad (7)$$

where an overdot represents material time derivative and

$$\mathbf{L}^e = \dot{\mathbf{F}}^e\mathbf{F}^{e-1}, \quad \mathbf{L}^g = \dot{\mathbf{F}}^g\mathbf{F}^{g-1} \quad (8)$$

The growth rate tensor \mathbf{L}^g is then decomposed as follows

$$\mathbf{L}^g = \frac{\Gamma}{3}\mathbf{I} + \text{dev}(\mathbf{L}^g), \quad \Gamma = \text{tr}(\mathbf{L}^g) = \frac{\dot{J}^g}{J^g} \quad (9)$$

where Γ is the growth rate and $\text{dev}(\cdot)$ represents the deviatoric operator². The deviatoric part of \mathbf{L}^g is associated with the directionality of growth in the dry reference space. When the volumetric growth rate Γ is zero, the growth directionality represents remodelling where the grown reference state is changing from processes like cellular rearrangement or changes in micro-structure.

3.2. Balance of mass

Mass balance of diffusing species can be written as

$$\dot{c}_R + \text{Div}(\mathbf{j}_R^M) = -\dot{\xi}_R \quad (10)$$

where ξ_R is the mass of diffusing species per unit volume of the dry reference configuration that has been consumed during growth and the concentration c_R is the mass of remaining diffusing species per unit dry reference volume. The vector \mathbf{j}_R^M is the referential diffusion flux written in units of mass of diffusing species per unit area per unit time. The mass balance equation eq. (10) can be rewritten in units of volume by multiplying it by Ω^f , the referential volume per unit mass of diffusing species³,

$$\Omega^f \dot{c}_R + \text{Div}(\mathbf{j}_R) = -\Omega^f \dot{\xi}_R, \quad \mathbf{j}_R = \Omega^f \mathbf{j}_R^M \quad (11)$$

where \mathbf{j}_R is the referential diffusion flux written in terms of volume of diffusing species per unit area per unit time. We can relate the remaining concentration of diffusing species per unit grown reference volume, c_g , to c_R as

$$c_R = c_g J^g \quad (12)$$

Swelling constraint: The change in J^s is assumed to arise entirely due to the change in the remaining diffusing species content, which yields the swelling constraint

$$\dot{J}^s = \Omega^f \dot{c}_g \quad (13)$$

² $\text{dev}(\mathbf{Z}) = \mathbf{Z} - \frac{1}{3}\text{tr}(\mathbf{Z})\mathbf{I}$

³In terms of the referential density (no elastic deformation) of diffusing species, ρ_0^f , we have the relation $\Omega^f = 1/\rho_0^f$.

Integration of eq. (13) along with the condition that the swelling ratio is unity when the solid is dry ($c_g = 0$) results in the following constraint,

$$J^s = 1 + \Omega^f c_g \quad (14)$$

Growth constraint: The consumption of the diffusing species supplies mass for the growth and leads to the following volumetric growth relation (also see Appendix A.1)

$$\dot{j}^g = \Omega^m \dot{\xi}_R \quad (15)$$

where Ω^m is the referential volume per unit mass of the solid matrix ($\Omega^m = 1/\rho_0^m$). The integrated form of eq. (15) reads

$$J^g = 1 + \Omega^m \xi_R \quad (16)$$

where the growth volume ratio is unity when no diffusing species has been consumed ($J^g = 1$ when $\xi_R = 0$). The constraint eq. (16) ensures mass balance during species conversion.

The eqs. (12), (13) and (15) can be used to rewrite eq. (11) as

$$J^g j^s + \dot{j}^g \left(J^s - 1 + \frac{\Omega^f}{\Omega^m} \right) + \text{Div}(\mathbf{j}_R) = 0 \quad (17)$$

The eqs. (14), (16) and (17) together ensure mass balance. Since the density of solid matrix is typically close to the density of the fluid components in our systems of interest, here we assume isochoric conversion of the diffusing species into solid so that $\Omega^f = \Omega^m = \Omega$. Under this assumption, eq. (17) simplifies to

$$J^g j^s + J^s \dot{j}^g + \text{Div}(\mathbf{j}_R) = 0 \quad (18)$$

See Appendix A.4 for the general version of the theory for non-isochoric species conversion.

3.3. Mechanical equilibrium

Let $\mathbf{T}(\mathbf{x}, t)$ and $\mathbf{S}(\mathbf{X}, t)$ denote the Cauchy and Piola stress tensor fields, respectively. Since swelling and growth are usually much slower than the mechanical response of the body, we ignore the momentum arising from swelling-growth. Mechanical equilibrium in the absence of body forces and inertial effects requires that (see also Ambrosi and Mollica (2004); Xue et al. (2016))

$$\text{div } \mathbf{T} = \mathbf{0}, \quad \mathbf{T} = \mathbf{T}^T \quad (19)$$

and equivalently that

$$\text{Div } \mathbf{S} = \mathbf{0}, \quad \mathbf{S}\mathbf{F}^T = \mathbf{F}\mathbf{S}^T, \quad \text{where } \mathbf{S} = J\mathbf{T}\mathbf{F}^{-T} \quad (20)$$

3.4. Dissipation inequality

Under isothermal conditions and in absence of body forces, the first two laws of thermodynamics collapse into the following free energy imbalance equation over any material subregion P

in the body (see Appendix A.2)

$$\int_{\mathbf{P}} \dot{\psi}_R dV_R \leq \int_{\partial\mathbf{P}} (\mathbf{S}\mathbf{n}_R) \cdot \dot{\boldsymbol{\varphi}} dA_R + \int_{\partial\mathbf{P}} \mu(-\mathbf{j}_R \cdot \mathbf{n}_R) dA_R \quad (21)$$

where ψ_R is the Helmholtz free energy per unit dry reference volume of the fluid-solid continuum within the dry material region \mathbf{P} and μ is the chemical potential of the diffusing species⁴. Localizing eq. (21), while employing eq. (18) yields the local dissipation inequality (see Appendix A.2)

$$\mathbf{S} \cdot \dot{\mathbf{F}} + \mu(J^g J^s + J^s J^g) - \mathbf{j}_R \cdot \nabla \mu - \dot{\psi}_R \geq 0 \quad (22)$$

It can be shown using (7) that (see Appendix A.3)

$$\mathbf{S} \cdot \dot{\mathbf{F}} = \frac{1}{2} J^s J^g \mathbf{T}^e \cdot \dot{\mathbf{C}}^e + J^g \mathbf{M}^{es} \cdot \mathbf{L}^g + \frac{J J^s}{3 J^s} \text{tr}(\mathbf{T}) \quad (23)$$

where the Mandel stress \mathbf{M}^{es} and the elastic second Piola stress \mathbf{T}^e are given by

$$\mathbf{M}^{es} = J^{es} \mathbf{F}^{esT} \mathbf{T} \mathbf{F}^{es-T}, \quad \mathbf{T}^e = J^e \mathbf{F}^{e-1} \mathbf{T} \mathbf{F}^{e-T} \quad (24)$$

Using eq. (23) and eq. (9)₂ in eq. (22), we arrive at the following form of the dissipation inequality,

$$J^g (\mathbf{M}^{es} + J^s \mu \mathbf{I}) \cdot \mathbf{L}^g + \frac{1}{2} J^s J^g \mathbf{T}^e \cdot \dot{\mathbf{C}}^e + \left(\mu + \frac{J^e}{3} \text{tr}(\mathbf{T}) \right) J^g J^s - \mathbf{j}_R \cdot \nabla \mu - \dot{\psi}_R \geq 0 \quad (25)$$

To be able to specify constitutive equations using the dissipation inequality, the form of the free energy is specified in the following section.

3.5. Free energy

We consider a free energy function of the form $\psi_R = \psi_R(J^g, J^s, \mathbf{C}^e)$, which we decompose as follows

$$\psi_R = J^g \psi_g(\mathbf{C}^e, J^s) + \mu_0^m \Omega^m \xi_R + \mu_0^f \Omega^f c_R \quad (26)$$

$$= J^g \psi_g(\mathbf{C}^e, J^s) + \mu_0^m (J^g - 1) + \mu_0^f J^g (J^s - 1) \quad (\text{Using (12), (14), (16)}) \quad (27)$$

$$\psi_g = \psi_g^{\text{mech}}(\mathbf{C}^e, J^s) + \psi_g^{\text{mix}}(J^s) \quad (28)$$

where

(i) μ_0^m is the reference chemical potential for the solid and $\mu_0^m \Omega^m \xi_R$ is the chemical energy of formed solid per unit dry reference volume.

(ii) μ_0^f is the reference chemical potential for the diffusing species and $\mu_0^f \Omega^f c_R$ is the biochemical energy of the diffusing species per unit dry reference volume. It represents the reference energy of the diffusing species with all its dissolved nutrients and growth factors.

⁴Typically the chemical potential μ is written in terms of energy per species unit (mole or molecule) since the flux is written in terms of species units per unit area per unit time, see for example Hong et al. (2008); Chester and Anand (2010). However, since the flux in this manuscript is written in terms of referential species volume per unit area per unit time, the chemical potential is in terms of energy per unit referential species volume.

- (iii) ψ_g^{mech} is the change in free energy due to the deformation of the solid, per unit grown reference volume.
- (iv) ψ_g^{mix} is the change in free energy due to mixing of the remaining diffusing species with the solid, per unit grown reference volume.

A specific form of the free energy is provided later. Differentiating eq. (26) and employing eqs. (9) and (12)–(15) yields the following equation,

$$\dot{\psi}_R = J^g \left(\psi_g + \mu_0^m + \mu_0^f (J^s - 1) \right) \mathbf{I} \cdot \mathbf{L}^g + J^g \frac{\partial \psi_g}{\partial \mathbf{C}^e} \cdot \dot{\mathbf{C}}^e + J^g \left(\mu_0^f + \frac{\partial \psi_g}{\partial J^s} \right) j^s \quad (29)$$

3.6. Constitutive response

Substituting eq. (29) in the dissipation inequality eq. (25) yields

$$J^g \mathbf{T}^g \cdot \mathbf{L}^g + \left(\frac{1}{2} J^s J^g \mathbf{T}^e - J^g \frac{\partial \psi_g}{\partial \mathbf{C}^e} \right) \cdot \dot{\mathbf{C}}^e + J^g \left(\mu + \frac{J^e}{3} \text{tr}(\mathbf{T}) - \frac{\partial \psi_g}{\partial J^s} - \mu_0^f \right) j^s - \mathbf{j}_R \cdot \nabla \mu \geq 0 \quad (30)$$

where \mathbf{T}^g is the driving stress conjugate to the growth deformation rate tensor \mathbf{L}^g , given by

$$\mathbf{T}^g = \mathbf{M}^{es} + \left(J^s \mu - \mu_0^m - \mu_0^f (J^s - 1) - \psi_g \right) \mathbf{I} \quad (31)$$

Employing the Coleman-Noll procedure we arrive at the following two constitutive equations for the elastic second Piola stress and chemical potential,

$$\mathbf{T}^e = \frac{2}{J^s} \frac{\partial \psi_g}{\partial \mathbf{C}^e}, \quad \mu = \mu_0^f + \frac{\partial \psi_g}{\partial J^s} - \frac{1}{3} J^e \text{tr}(\mathbf{T}), \quad (32)$$

respectively. We can then readily derive the constitutive equations for the Cauchy, Piola, and Mandel stresses using eqs. (1), (20) and (24) as

$$\mathbf{T} = 2 \frac{J^g}{J} \mathbf{F}^e \frac{\partial \psi_g}{\partial \mathbf{C}^e} \mathbf{F}^{eT}, \quad \mathbf{S} = 2 J^g \mathbf{F}^{es} \frac{\partial \psi_g}{\partial \mathbf{C}^{es}} \mathbf{F}^{g-T}, \quad \mathbf{M}^{es} = 2 \mathbf{C}^e \frac{\partial \psi_g}{\partial \mathbf{C}^e} \quad (33)$$

Further substituting eq. (32)₂ for the chemical potential in eq. (31) results in the following equation for the growth driving stress,

$$\mathbf{T}^g = \mathbf{M}^{es} + \left(\Delta \mu_0 + J^s \left(\frac{\partial \psi_g}{\partial J^s} - \frac{1}{3} J^e \text{tr}(\mathbf{T}) \right) - \psi_g \right) \mathbf{I} \quad (34)$$

where $\Delta \mu_0 = \mu_0^f - \mu_0^m$ is the energy associated with converting a unit (referential) volume of diffusing species to solid, henceforth referred to as conversion energy.

To ensure non-negative dissipation rate, we require the following residual inequality to be satisfied

$$J^g \mathbf{T}^g \cdot \mathbf{L}^g - \mathbf{j}_R \cdot \nabla \mu \geq 0 \quad (35)$$

We enforce the following inequalities to be independently satisfied,

$$\mathbf{T}^g \cdot \mathbf{L}^g \geq 0, \quad \mathbf{j}_R \cdot \nabla \mu \leq 0 \quad (36)$$

so that the dissipation inequality (35) is automatically enforced. We choose the following thermodynamically admissible prescription for the diffusion flux,

$$\mathbf{j}_R = -\mathbf{M}_{\text{mob}} \nabla \mu \quad (37)$$

where the mobility tensor \mathbf{M}_{mob} is positive semi-definite. The diffusion law in eq. (37) can be written in the current configuration as

$$\mathbf{j} = -\frac{\mathbf{F}\mathbf{M}_{\text{mob}}\mathbf{F}^T}{J} \text{grad } \mu \quad (38)$$

where $\mathbf{j} = \mathbf{F}\mathbf{j}^R/J$ is the diffusion flux in the current space such that $\mathbf{j} \cdot \mathbf{n} dA = \mathbf{j}_R \cdot \mathbf{n}_R dA_R$, and $\text{grad } (\cdot) = \mathbf{F}^{-T} \nabla (\cdot)$ is the Eulerian spatial gradient operator. The form of the mobility tensor is specified later in Section 4.4.

3.6.1. Growth kinetics

Following the previous constitutive prescriptions, we are left with the following inequality to be satisfied

$$\mathbf{T}^g \cdot \mathbf{L}^g = \Gamma \frac{\text{tr}(\mathbf{T}^g)}{3} + \text{dev}(\mathbf{T}^g) \cdot \text{dev}(\mathbf{L}^g) \geq 0 \quad (39)$$

where we used⁵ eq. (9) to examine the separate contributions of volumetric growth and growth directionality. Any prescription for \mathbf{L}^g that satisfies this inequality is a thermodynamically admissible growth law. We enforce the following inequalities separately,

$$\Gamma \frac{\text{tr}(\mathbf{T}^g)}{3} \geq 0, \quad \text{dev}(\mathbf{T}^g) \cdot \text{dev}(\mathbf{L}^g) \geq 0 \quad (40)$$

such that the inequality in eq. (39) is automatically satisfied.

Volumetric growth rate: Using the expression for \mathbf{T}^g in eq. (34) along with eq. (24)₁, we can write eq. (40)₁ as

$$\Gamma f_g \geq 0, \quad f_g = \frac{\text{tr}(\mathbf{T}^g)}{3} = \Delta \mu_0 + J^s \frac{\partial \psi_g}{\partial J^s} - \psi_g \quad (41)$$

where f_g is the driving stress for volumetric growth. Any thermodynamically admissible growth law for the volumetric growth rate can be prescribed as follows

$$\Gamma = \hat{\Gamma}(f_g) \quad \text{such that} \quad \hat{\Gamma}(f_g) f_g \geq 0 \quad (42)$$

⁵Note the identity $\mathbf{Y} \cdot \text{dev}(\mathbf{Z}) = \text{dev}(\mathbf{Y}) \cdot \text{dev}(\mathbf{Z})$

Recalling that $\psi_g = \psi_g^{\text{mech}} + \psi_g^{\text{mix}}$, the driving stress f_g in eq. (41)₂ can be decomposed as follows

$$f_g = \Delta\mu_0 + f_g^{\text{mix}} + f_g^{\text{mech}} \quad (43)$$

where f_g^{mix} and f_g^{mech} are the parts of the driving stress that arise from the mixing free energy and mechanical free energy respectively,

$$f_g^{\text{mix}} = J^s \frac{\partial \psi_g^{\text{mix}}}{\partial J^s} - \psi_g^{\text{mix}}, \quad f_g^{\text{mech}} = J^s \frac{\partial \psi_g^{\text{mech}}}{\partial J^s} - \psi_g^{\text{mech}} \quad (44)$$

Growth directionality evolution: Similarly using the expression for \mathbf{T}^g in eq. (34), we can write eq. (40)₂ as

$$\text{dev}(\mathbf{M}^{es}) \cdot \text{dev}(\mathbf{L}^g) \geq 0 \quad (45)$$

Any thermodynamically admissible evolution law for the growth directionality can thus be prescribed as follows

$$\text{dev}(\mathbf{L}^g) = \hat{\mathbf{f}}(\mathbf{M}^{es}) \quad \text{such that} \quad \hat{\mathbf{f}}(\mathbf{M}^{es}) \cdot \text{dev}(\mathbf{M}^{es}) \geq 0 \quad (46)$$

Therefore, the Mandel stress drives growth directionality. Morphogenesis, the process by which the growing body acquires its shape, can arise from both spatially varying growth rates and evolution of growth directionality. When the growth rate is spatially uniform, morphogenesis would be driven solely by the Mandel stress.

In Section 4.3, we will specify the forms of the evolution functions $\hat{\Gamma}(f_g)$ and $\hat{\mathbf{f}}(\mathbf{M}^{es})$ to obtain specialized forms of the growth evolution laws in eqs. (42) and (46).

3.7. Summary of formulation and boundary conditions

The governing equations of the swelling-growth theory for isochoric conversion of diffusing species to solid are summarized below. See Appendix A.4 for the general equations for non-isochoric species conversion.

Governing equations in \mathcal{B}^R

$$\text{Mechanical equilibrium :} \quad \text{Div } \mathbf{S} = \mathbf{0}, \quad \mathbf{S} = 2J^g \mathbf{F}^{es} \frac{\partial \psi_g}{\partial \mathbf{C}^{es}} \mathbf{F}^{g-T} \quad (47)$$

$$\text{Mass balance :} \quad J^g \dot{J}^s + J^s \dot{J}^g = \text{Div}(\mathbf{M}_{\text{mob}} \nabla \mu) \quad (48)$$

$$\text{Constitutive equations :} \quad \mu = \mu_0^f + \frac{\partial \psi_g}{\partial J^s} - \frac{1}{3} J^e \text{tr}(\mathbf{T}), \quad \mathbf{T} = 2 \frac{J^g}{J} \mathbf{F}^e \frac{\partial \psi_g}{\partial \mathbf{C}^e} \mathbf{F}^{eT} \quad (49)$$

$$\text{Kinetic law for volumetric growth :} \quad \frac{\dot{J}^g}{J^g} = \hat{\Gamma}(f_g), \quad \hat{\Gamma}(f_g) f_g \geq 0 \quad (50)$$

$$\text{Kinetic law for growth directionality :} \quad \text{dev}(\mathbf{L}^g) = \hat{\mathbf{f}}(\mathbf{M}^{es}), \quad \hat{\mathbf{f}}(\mathbf{M}^{es}) \cdot \text{dev}(\mathbf{M}^{es}) \geq 0 \quad (51)$$

To complete the theory development, initial and boundary conditions need to be prescribed. We consider the following sets of complementary subsurfaces of the boundary $\partial \mathcal{B}^R$: $\{\partial \mathcal{B}_t^R, \partial \mathcal{B}_x^R\}$, $\{\partial \mathcal{B}_j^R, \partial \mathcal{B}_\mu^R\}$, where any two subsurfaces $\partial \mathcal{B}_a^R$ and $\partial \mathcal{B}_b^R$ are complementary if $\partial \mathcal{B}_a^R \cup \partial \mathcal{B}_b^R = \partial \mathcal{B}^R$ and $\partial \mathcal{B}_a^R \cap \partial \mathcal{B}_b^R = \emptyset$. Then for a time interval $t \in [0, t_f]$ we consider the following boundary and

initial conditions.

Boundary conditions

$$\text{Traction :} \quad \mathbf{S}\mathbf{n}_R = \check{\mathbf{s}} \quad \text{on } \partial\mathcal{B}_t^R \times [0, t_f] \quad (52)$$

$$\text{Position :} \quad \mathbf{x}(\mathbf{X}) = \check{\mathbf{x}} \quad \text{on } \partial\mathcal{B}_x^R \times [0, t_f] \quad (53)$$

$$\text{Diffusion flux :} \quad -(\mathbf{M}_{\text{mob}}\nabla\mu) \cdot \mathbf{n}_R = \check{j} \quad \text{on } \partial\mathcal{B}_j^R \times [0, t_f] \quad (54)$$

$$\text{Chemical potential :} \quad \mu = \check{\mu} \quad \text{on } \partial\mathcal{B}_\mu^R \times [0, t_f] \quad (55)$$

with $\check{\mathbf{s}}, \check{\mathbf{x}}, \check{j}, \check{\mu}$ being prescribed functions that depend on \mathbf{X} and t .

Initial conditions

$$\mu(\mathbf{X}, 0) = \mu_0(\mathbf{X}), \quad \mathbf{F}^g(\mathbf{X}, 0) = \mathbf{F}_0^g(\mathbf{X}) \quad (56)$$

where μ_0 and \mathbf{F}_0^g are prescribed functions. For the analysis in this manuscript, we set $\mathbf{F}_0^g(\mathbf{X}) = \mathbf{I}$.

This completes the development of the large deformation swelling-growth theory. It is important to note that setting $\mathbf{F}^g = \mathbf{I}$ recovers nonlinear poroelastic theories. In the next section, we will choose specific constitutive equations to specialize our theory and also write the dimensionless form of the governing equations.

4. Specific constitutive equations and dimensionless formulation

In this section, we specialize the equations of the swelling-growth theory developed in the previous section by choosing specific forms for the free energy, mobility tensor, and growth evolution laws.

4.1. Mechanical free energy

We limit our attention to isotropic materials. The following form is chosen for the mechanical free energy

$$\psi_g^{\text{mech}}(\mathbf{C}^e, J^s) = \frac{G}{2} \left((J^s)^{\frac{2}{3}} \text{tr}(\mathbf{C}^e) - 3 - 2 \ln(J^{es}) \right) + \frac{K}{2} (\ln J^e)^2, \quad J^e = \sqrt{\det(\mathbf{C}^e)} \quad (57)$$

where G and K are the linear shear modulus and the bulk modulus of the dry solid respectively. The first term in eq. (57) is the entropic free energy change due to mechanical stretching of the polymer network, given by classical statistical mechanics model of rubber elasticity (Treloar, 1975). The second term is the energetic component of free energy change due to compressibility of the hydrogel, as also used in Chester and Anand (2011). Note that in the absence of swelling, the mechanical free energy is essentially a compressible neo-Hookean model. While there are better tailored free energy functions with more parameters to describe biological tissues, this is a simple first choice for modelling of soft polymers or tissues (for example see tumor modelling in Xue et al. (2016)).

Hence the Cauchy and Mandel stresses are derived using eqs. (33) and (57) as

$$\mathbf{T} = \frac{1}{J^{es}} (G (\mathbf{B}^{es} - \mathbf{I}) + K(\ln J^e)\mathbf{I}), \quad \mathbf{M}^{es} = G (\mathbf{C}^{es} - \mathbf{I}) + K(\ln J^e)\mathbf{I} \quad (58)$$

The following derivative is also readily derived,

$$\frac{\partial \psi_g^{\text{mech}}}{\partial J^s} = \frac{G}{3J^s} (\text{tr}(\mathbf{C}^{es}) - 3) \quad (59)$$

4.2. Mixing free energy

The free energy of mixing is taken to be (Flory, 1942; Huggins, 1941)

$$\psi_g^{\text{mix}} = \frac{\mu^*}{\phi} ((1 - \phi) \ln(1 - \phi) + \chi \phi(1 - \phi)) \quad \text{where} \quad \mu^* = \frac{k_B T}{\omega^f}, \quad \omega^f = M^f \Omega^f \quad (60)$$

where ω^f and M^f are the molecular volume and mass respectively of the diffusing species, k_B is the Boltzmann constant, T is the constant temperature, and χ is the Flory–Huggins interaction parameter. The scalar μ^* will later be used as a characteristic scaling value for the chemical potential when developing the dimensionless version of the theory. The interaction parameter χ represents the dis-affinity between the solid and the diffusing species; the larger the χ the smaller the swelling ratio at diffusion equilibrium (at a fixed growth state). For $\chi \leq 0.5$ the minimum of ψ_g^{mix} occurs at $\phi \rightarrow 0$ which means that in the absence of mechanical free energy (say $G, K \rightarrow 0$), the solid would want to keep swelling till $J^s \rightarrow \infty$ (i.e. $\phi \rightarrow 0$). However for $\chi > 0.5$, the minimum of ψ_g^{mix} occurs at $0 < \phi < 1$ so that even in the absence of mechanical energy, the solid would swell to a finite swelling ratio at diffusion equilibrium. Using the definition of solid volume fraction ϕ from eq. (5) in eq. (60), the following derivative is readily obtained

$$\frac{\partial \psi_g^{\text{mix}}}{\partial J^s} = \mu^{\text{mix}}(\phi) = \mu^* (\ln(1 - \phi) + \phi + \chi \phi^2) \quad (61)$$

where we have defined an auxiliary function $\mu^{\text{mix}}(\phi)$ for later convenience.

Using eqs. (6), (28), (32), (58), (59) and (61), we obtain the following equation for the chemical potential

$$\mu = \mu_0^f + \mu^{\text{mix}}(\phi) - K \ln(J^e) \phi \quad (62)$$

4.3. Growth evolution

Guided by the inequality in eq. (42), we choose a piece-wise linear form of the volumetric growth law that enforces irreversibility of species conversion⁶,

$$\Gamma = \begin{cases} k_g f_g, & \text{if } f_g \geq 0 \\ 0, & \text{if } f_g < 0 \end{cases} \quad (63)$$

⁶While technically cells can die and decompose back into the diffusing components, the associated processes and kinetics are usually different from that of growth and we avoid such considerations here.

where k_g is a growth constant. Further, using eqs. (44), (57) and (59)–(61), we arrive at the following expressions for different components of f_g in eq. (43),

$$f_g^{\text{mech}} = G \left(\ln(J^{es}) - \frac{1}{6} (\text{tr}(\mathbf{C}^{es}) - 3) \right) - \frac{K}{2} (\ln(J^e))^2 \quad (64)$$

$$f_g^{\text{mix}}(\phi) = \mu^* (1 + \ln(1 - \phi) + \chi(2\phi - 1)) \quad (65)$$

Similarly, guided by the inequality in eq. (46), we choose the following linear evolution law for the growth directionality

$$\text{dev}(\mathbf{L}^g) = \frac{k_g}{3} \text{dev}(\mathbf{M}^{es}) = \frac{k_g G}{3} \text{dev}(\mathbf{C}^{es}) \quad (66)$$

where for simplicity we have chosen the same rate parameter k_g as for the volumetric growth evolution law and have used eq. (58)₂ for the Mandel stress. When $f_g \geq 0$, the evolution laws eqs. (63) and (66) can be combined and written as $3\mathbf{L}^g = k_g \mathbf{T}^g$.

4.4. Mobility tensor

The diffusion is assumed to be modelled by the following Eulerian law

$$\mathbf{j} = -\hat{h}(J^s) m^* \text{grad } \mu, \quad m^* = \frac{D}{\mu^*} \quad (67)$$

where D is the diffusion coefficient, m^* is the characteristic scaling value for the mobility, and $\hat{h}(J^s)$ describes the dependence of the mobility in the current space on swelling. Using eq. (38), the associated mobility tensor is readily shown to be

$$\mathbf{M}^{\text{mob}} = \hat{h}(J^s) m^* J \mathbf{C}^{-1} \quad \text{where } \mathbf{C} = \mathbf{F}^T \mathbf{F} \quad (68)$$

Different works in the literature have assumed different monotonically increasing functional forms for \hat{h} (Baek and Srinivasa, 2004; Hong et al., 2008; Duda et al., 2010; Chester and Anand, 2011; Abi-Akl et al., 2019). For example Hong et al. (2008) employed $\hat{h} = J^s - 1$ while Abi-Akl et al. (2019) chose $\hat{h} = (J^s - 1)/J^s$. However in the absence of any experimental evidence to choose a particular functional form, here we choose $\hat{h} = 1$ which suffices to demonstrate all the relevant physics while avoiding zero mobility in the dry state. Further, we note that different choices for \hat{h} preserve the conclusions in this manuscript.

4.5. Dimensionless equations and approximate limits

In this section, a dimensionless version of the theory is developed which aids greatly with the analysis in later sections and in making suitable approximations under different limiting conditions. We first define the following dimensionless operations and quantities,

$$\overline{\text{Div}} = L^* \text{Div}, \quad \overline{\nabla} = L^* \nabla, \quad \bar{\mu} = \frac{\mu}{\mu^*}, \quad \overline{\mathbf{M}}_{\text{mob}} = \frac{\mathbf{M}^{\text{mob}}}{m^*}, \quad \bar{t}_d = \frac{t}{\tau_d} \quad (69)$$

where L^* is a characteristic length scale and $\tau_d = L^{*2}/D$ is the associated diffusion timescale. Using the definitions from eq. (69) along with eq. (68) and eq. (67)₂ in eq. (48) yields the following dimensionless diffusion-consumption equation,

$$J^g \frac{dJ^s}{d\bar{t}_d} + J^s \frac{dJ^g}{d\bar{t}_d} = \overline{\text{Div}} (\overline{\mathbf{M}}_{\text{mob}} \overline{\nabla} \bar{\mu}), \quad \overline{\mathbf{M}}_{\text{mob}} = J\mathbf{C}^{-1} \quad (70)$$

The dimensionless counterpart for the constitutive equation (62) for chemical potential is

$$\bar{\mu} = \bar{\mu}_0^f + \bar{\mu}^{\text{mix}}(\phi) - \left(\frac{K}{G}\right) \left(\frac{G}{\mu^*}\right) \ln(J^e)\phi \quad \text{where} \quad \bar{\mu}_0^f = \frac{\mu_0^f}{\mu^*}, \quad \bar{\mu}^{\text{mix}} = \frac{\mu^{\text{mix}}}{\mu^*} \quad (71)$$

The Cauchy stress in eq. (58) is non-dimensionalized using the shear modulus G as follows,

$$\bar{\mathbf{T}} = \frac{\mathbf{T}}{G} = \frac{1}{J^{es}} (\mathbf{B}^{es} - \mathbf{I}) + \left(\frac{K}{G}\right) \frac{\ln J^e}{J^{es}} \mathbf{I} \quad (72)$$

where K/G is a measure of the compressibility of the solid. A perfectly incompressible version of theory is developed in Appendix B where $K/G \rightarrow \infty$ such that $J^e \rightarrow 1$. The dimensionless version of the mechanical equilibrium equation (20) is written as

$$\overline{\text{Div}} \bar{\mathbf{S}} = \mathbf{0} \quad \text{where} \quad \bar{\mathbf{S}} = \frac{\mathbf{S}}{G} = J\bar{\mathbf{T}}\mathbf{F}^{-T} \quad (73)$$

Defining the following additional quantities,

$$\bar{f}_g = \frac{f_g}{\mu^*}, \quad \tau_g = \frac{1}{k_g \mu^* \bar{f}_g^*}, \quad \bar{t}_g = \frac{t}{\tau_g}, \quad \bar{\Gamma} = \tau_g \Gamma = \frac{1}{J^g} \frac{dJ^g}{d\bar{t}_g} \quad (74)$$

where τ_g is a characteristic timescale of growth and \bar{f}_g^* is a dimensionless constant chosen to normalize the growth law, we can rewrite the volumetric growth law (63) in dimensionless form as

$$\bar{\Gamma} = \begin{cases} \bar{f}_g / \bar{f}_g^*, & \text{if } \bar{f}_g \geq 0 \\ 0, & \text{if } \bar{f}_g < 0 \end{cases} \quad (75)$$

where $\bar{\Gamma}$ is the dimensionless growth rate. Non-dimensionalizing eqs. (43), (64) and (65) using μ^* yields

$$\bar{f}_g = \Delta \bar{\mu}_0 + \bar{f}_g^{\text{mix}} + \bar{f}_g^{\text{mech}} \quad (76)$$

where $\Delta \bar{\mu}_0 = \Delta \mu_0 / \mu^*$ and

$$\bar{f}_g^{\text{mix}}(\phi) = \frac{f_g^{\text{mix}}(\phi)}{\mu^*} = 1 + \ln(1 - \phi) + \chi(2\phi - 1), \quad (77)$$

$$\bar{f}_g^{\text{mech}} = \frac{f_g^{\text{mech}}}{\mu^*} = \frac{G}{\mu^*} \left(\ln(J^{es}) - \frac{1}{2} \left(\frac{K}{G}\right) (\ln(J^e))^2 - \frac{1}{6} (\text{tr}(\mathbf{C}^{es}) - 3) \right) \quad (78)$$

The evolution equation for growth directionality eq. (66) can be written in dimensionless form as

$$\text{dev}(\bar{\mathbf{L}}^g) = \frac{1}{3} \left(\frac{G}{\mu^*} \right) \frac{\text{dev}(\bar{\mathbf{M}}^{es})}{\bar{f}_g^*} = \frac{1}{3} \left(\frac{G}{\mu^*} \right) \frac{\text{dev}(\mathbf{C}^{es})}{\bar{f}_g^*} \quad (79)$$

where $\bar{\mathbf{M}}^{es} = \mathbf{M}^{es}/G$ and $\bar{\mathbf{L}}^g = \tau_g \mathbf{L}^g$.

Note from eqs. (58) and (79) that for the growth to completely stop ($\mathbf{L}^g = \mathbf{0}$), the stress state \mathbf{T} necessarily needs to be hydrostatic. This is a consequence of the fact that there is no inherent directionality for swelling or species conversion which are the growth driving mechanisms in our theory (all the non-stress terms in the driving stress \mathbf{T}^g are hydrostatic in eq. (34)). However, in the limit $G/\mu^* \rightarrow 0$, the system can stop growing even at non-hydrostatic stress states. Essentially, in this limit, the growth stops once the volumetric growth halts as the remodelling is slow at the timescale of volumetric growth.

For our soft growing systems of interest, the value of the shear modulus G is typically low, ~ 1 kPa (Garteiser et al., 2012; Zhang et al., 2021), while the value of μ^* is high for typical swelling fluids at room temperature, ~ 10 -100 MPa (Hong et al., 2008; Chester and Anand, 2010). Thus the value of the dimensionless parameter G/μ^* is very small ($\sim 1e^{-5}$ - $1e^{-4}$). Consequently it can be inferred from eq. (79) that the growth directionality will be nearly isotropic. Thus if $\mathbf{F}_0^g = \mathbf{I}$, the growth tensor \mathbf{F}^g continues to remain nearly spherical/isotropic during growth unless the dimensionless Mandel stress reaches large and highly non-spherical values. *This explains why the assumption of isotropic growth, which is commonly used in the literature for soft growing systems (Ambrosi and Mollica, 2002, 2004; Kim et al., 2011; Köpf and Pismen, 2013; Kuhl, 2014), works well.* Note that this is a consequence of our constitutive choice of same growth constant k_g to describe the evolution of both volumetric growth in eq. (63) and growth directionality in eq. (66), combined with the fact that $\text{tr}(\mathbf{T}_g) \sim \mu^*$ (when $\mu^* \gg G$ and dimensionless stresses are not very large non-spherical values) whereas $\text{dev}(\mathbf{T}_g) \sim G$. However, more generally growth laws can be specified with different growth constants for the volumetric and deviatoric parts of the growth rate tensor (for example if cellular rearrangement is much faster than cell division in a particular growing system) which can lead to more anisotropic growth evolution. Further, it can be shown from eqs. (77) and (78) that $\bar{f}_g^{\text{mix}} \gg \bar{f}_g^{\text{mech}}$ for small G/μ^* as long as the dimensionless stresses are not very large⁷. Thus the dimensionless driving stress for volumetric growth can typically be approximated very well as

$$\bar{f}_g \approx \Delta\bar{\mu}_0 + \bar{f}_g^{\text{mix}}(\phi) \quad (80)$$

which is primarily a function of $\Delta\bar{\mu}_0$ (dimensionless conversion energy), and the solid volume fraction, or equivalently the swelling ratio - recall eq. (5). Thus the swelling can be seen to be an important driver of growth. The approximation also allows us to examine the driving stress and make several key inferences before even solving boundary value problems, in Section 5.1.

⁷Note that while the term $\frac{K}{G} \rightarrow \infty$ in the incompressible limit, the term $\frac{K}{G} (\ln(J^e))^2$ in \bar{f}_g^{mech} (eq. (78)) still approaches zero. See Appendix B and eq. (B.7) for expression of f_g^{mech} in the perfectly incompressible limit. Numerical simulations in Section 5 for the slightly compressible case also confirm $\bar{f}_g^{\text{mix}} \gg \bar{f}_g^{\text{mech}}$.

Finally, using eqs. (74)₄, (75), and the definitions of \bar{t}_d and \bar{t}_g from eq. (69) and eq. (74) respectively, we can rewrite eq. (70) as follows

$$J^g \frac{dJ^s}{d\bar{t}_d} + J^s J^g \bar{\Gamma} \left(\frac{\tau_d}{\tau_g} \right) = \overline{\text{Div}} (\overline{\mathbf{M}}_{\text{mob}} \overline{\nabla} \bar{\mu}) \quad (81)$$

In many growing systems, due to typically large growth timescales relative to small diffusion timescales (due to small sizes), $\tau_g \gg \tau_d$. Thus at the timescale of growth, the diffusion is often assumed to be equilibrated (Greenspan, 1972; Preziosi, 2003; Ambrosi and Mollica, 2002, 2004), and the following equilibrated version of the diffusion-consumption equation can be used

$$J^s J^g \bar{\Gamma} \left(\frac{\tau_d}{\tau_g} \right) = \overline{\text{Div}} (\overline{\mathbf{M}}_{\text{mob}} \overline{\nabla} \bar{\mu}) \quad (82)$$

In this limit, the net flux of diffusing species (right hand side) is being matched exactly by the consumption for growth (left hand side). Note that for a given growth rate $\bar{\Gamma}$, the larger the body grows (larger $J^g J^s$), the larger the consumption term. For the tumor growth experiments discussed in Section 2, this is what causes the equilibrium swelling profile (or equivalently concentration profile using eq. (14)) to drop with time inside the tumor for free growth, resulting in reduced growth rates. When the equilibrated equation (82) is used, the initial condition for chemical potential field in eq. (56) need not be supplied.

When we are not interested in diffusion-consumption limitations due to large growth sizes and instead want to isolate the effect of applied stresses, we can focus on the limit $\tau_g/\tau_d \rightarrow \infty$ where the diffusion is infinitely faster than growth. In this limit, the left hand side of eq. (82) becomes zero and solutions where all spatial fields are uniform are possible for suitable boundary value problems, allowing for analytical tractability. We analyze this limit while enforcing perfect incompressibility ($K/G \rightarrow \infty, J^e \rightarrow 1$) in Section 5.2. The results are useful in establishing the effects of mechanical constraints on swelling-growth and subsequently in analyzing and explaining the results when we consider added diffusion-consumption limitations (finite τ_g/τ_d). In the following section, we will use the developed swelling-growth theory to study relevant boundary value problems and model experiments of growing tumors and bacterial biofilms.

5. Analysis and results

This section is organized as follows: We first examine the growth driving stress in the limit $G/\mu^* \rightarrow 0$ in Section 5.1 and establish notions of a critical swelling ratio and critical conversion energy that can halt growth. Following this, in Section 5.2 we focus on the effects of applied stresses in the absence of diffusion-consumption limitations by studying uniform swelling-growth that emerges in the limit of infinitely fast diffusion ($\tau_g/\tau_d \rightarrow \infty$) and uniform applied pressure. By linking the swelling ratio to the applied pressure, we establish a free swelling ratio in the absence of stresses and a homeostatic pressure associated with the critical swelling ratio. In Section 5.2.1, we demonstrate the above established concepts by studying the problem of uniform swelling-growth against mechanical confinement in the infinitely fast diffusion limit. To account for diffusion-consumption effects (finite τ_g/τ_d), which entails spatially varying field variables, we formulate a spherically symmetric boundary value problem in Section 5.3. The formulation is

used to study the case of free growth in Section 5.4 and the case of uniform applied pressure in Section 5.5. Finally, the theory is used to model experimental results of growing tumors in Section 5.6 and of bacterial biofilms in Section 5.7.

5.1. Growth driving stress

We consider the limit $G/\mu^* \rightarrow 0$ (which is the case for our soft growing systems of interest as discussed in Section 4.5). In this limit, the growth directionality evolution equation (79) becomes trivial and enforces isotropy of growth so that $\mathbf{F}^g = J^g \mathbf{I}$. Using eq. (75) for the growth rate evolution, the growth process is now primarily determined by the dimensionless driving stress \bar{f}_g . In the limit $G/\mu^* \rightarrow 0$, we have

$$\bar{f}_g = \Delta\bar{\mu}_0 + \bar{f}_g^{\text{mix}}(\phi) \quad (83)$$

where $\bar{f}_g^{\text{mix}}(\phi)$ is defined in eq. (77) and ϕ is related to the swelling ratio J^s through eq. (5). Thus, any dependence of the growth on applied stresses and diffusion-consumption effects appears through the swelling ratio J^s (note that J^s depends on the mechanical equilibrium and diffusion-consumption equations in Section 3.7). We first consider $\Delta\bar{\mu}_0 = 0$ (no contribution from species conversion) and examine the dependence of the dimensionless driving stress \bar{f}_g on the swelling ratio J^s and the Flory-Huggins interaction parameter χ . Note that non-zero values of $\Delta\bar{\mu}_0$ will simply shift \bar{f}_g by a constant and not affect its qualitative dependence on J^s and χ .

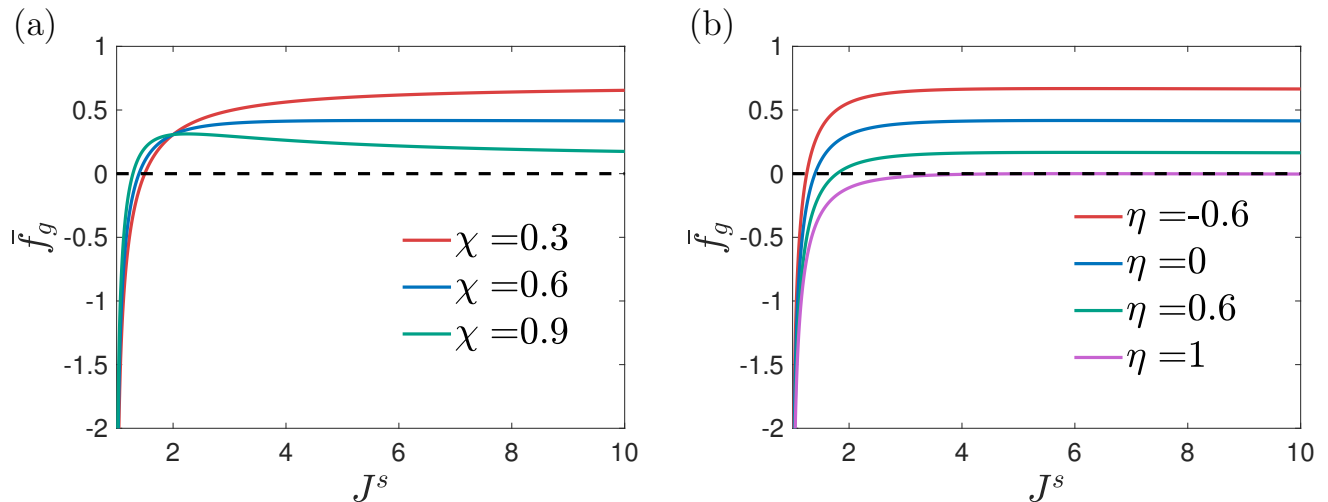


Figure 3: Dimensionless driving stress for volumetric growth, \bar{f}_g , as a function of the swelling ratio in the limit $G/\mu^* \rightarrow 0$. (a) Plots of \bar{f}_g for different values of Flory-Huggins interaction parameter χ and zero conversion energy ($\Delta\mu_0 = 0$). (b) Plots of \bar{f}_g for different values of the conversion energy ratio η for fixed representative value of $\chi = 0.6$.

Dependence on J^s : The dimensionless driving stress \bar{f}_g is plotted as a function of the swelling ratio J^s when $\Delta\bar{\mu}_0 = 0$ in Figure 3(a), for different values of the Flory-Huggins interaction parameter χ . This plot shows the functional dependence of \bar{f}_g as a function of the swelling ratio (or equivalently concentration of diffusing species, recall eq. (14)) in the absence of any conversion energy. It can be seen that generally higher J^s leads to a larger driving stress for volumetric growth and that the driving stress saturates at high values of J^s . There exists a

critical value of swelling ratio, J_c^s , below which $\bar{f}_g < 0$. Based on our growth law in eq. (75), this implies that growth halts for $J^s < J_c^s$, while for $J^s > J_c^s$, the growth rate linearly scales with \bar{f}_g . Thus our theory already offers a kinetic basis for the experimentally observed dependence of the growth rate on concentration of diffusing species, wherein the growth rate increases with concentration, saturates at high values and halts below a critical value.

Effect of χ : The influence of χ on the driving stress is also shown in Figure 3(a). The asymptotic value of \bar{f}_g^{mix} as $J^s \rightarrow \infty$ is given by $1 - \chi$ and thus decreases for increasing χ (larger dis-affinity between the solid and diffusing species). For $\chi < 0.5$, \bar{f}_g is a monotonically increasing function of J^s and reaches its maximum value at $J_{\text{max}}^s \rightarrow \infty$. For $\chi \geq 0.5$, the driving stress \bar{f}_g monotonically increases with J^s till it reaches a maximum value at $J^s = J_{\text{max}}^s = 2\chi/(2\chi - 1)$ and subsequently decreases to its asymptotic value as $J^s \rightarrow \infty$. This decrease is typically mild, except for very high values of χ (such as $\chi = 0.9$ in Figure 3(a)), which are typically unphysical and represent extreme dis-affinity between solid and diffusing species. The maximum value of the driving stress \bar{f}_g^{mix} is derived to write

$$\max_{1 \leq J^s < \infty} \bar{f}_g^{\text{mix}}(J^s) = \begin{cases} \chi - \ln(2\chi), & \text{for } \chi > 0.5 \\ 1 - \chi, & \text{for } 0 < \chi < 0.5 \end{cases} \quad (84)$$

which is always a positive value (as also seen in Figure 3(a)).

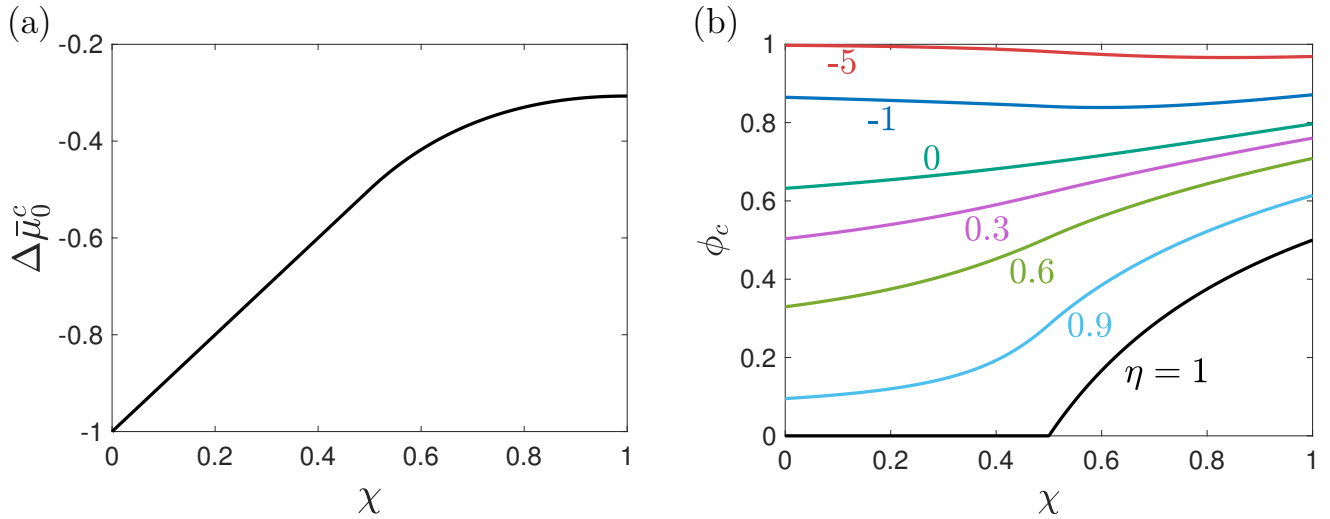


Figure 4: (a) Plot of the dimensionless critical conversion energy that prohibits volumetric growth for any swelling ratio as a function of the Flory-Huggins interaction parameter χ in the limit $G/\mu^* \rightarrow 0$. (b) Plot of the critical solid value fraction ϕ_c , which is the value of solid volume fraction that stops growth ($\bar{f}_g(\phi_c) = 0$), versus χ for various values of the conversion energy ratio η , in the limit $G/\mu^* \rightarrow 0$.

Effect of $\Delta\bar{\mu}_0$: Now we consider the effect of non-zero dimensionless conversion energy $\Delta\bar{\mu}_0$. A positive value of $\Delta\bar{\mu}_0$ corresponds to remaining energy after species conversion that accelerates growth whereas a negative value corresponds to an energy penalty that deters growth. We can define a critical dimensionless conversion energy, $\Delta\bar{\mu}_0^c$, as the maximum value of $\Delta\bar{\mu}_0$ such that

$\bar{f}_g \leq 0$ for all values of J^s . Using eq. (83), we can write

$$\Delta\bar{\mu}_0^c = - \max_{1 \leq J^s < \infty} \bar{f}_g^{\text{mix}}(J^s) \quad (85)$$

When $\Delta\bar{\mu}_0 < \Delta\bar{\mu}_0^c$, growth is not possible irrespective of the swelling ratio since $\bar{f}_g \leq 0$ for any value of the swelling ratio J^s . Using eqs. (84) and (85), the critical dimensionless conversion energy for growth, $\Delta\bar{\mu}_0^c$, is plotted in Figure 4(a) as a function of χ . The value of $\Delta\bar{\mu}_0^c$ is always negative, thus there is a maximum energy penalty for the species conversion, above which growth will always be unfavourable no matter the swelling. The larger the χ , the smaller the conversion penalty required to stop growth. We can then define a conversion energy ratio $\eta = \Delta\bar{\mu}_0/\Delta\bar{\mu}_0^c$ such that $\eta \leq 1$ for growth to be feasible. A plot of \bar{f}_g as a function of J^s for varying values of η is plotted in Figure 3(b) for $\chi = 0.6$. The larger the value of η , the smaller the dimensionless driving stress for any given J^s , and for $\eta = 1$, the growth is seen to be always unfeasible. Since $\Delta\bar{\mu}_0^c < 0$, a positive value of η corresponds to an energy penalty which is seen to deter growth (reduced \bar{f}_g) compared to $\eta = 0$ while a negative value corresponds to excess energy that can be seen to accelerate growth.

Critical swelling ratio dependence: As noted earlier, there exists a critical value of swelling ratio, J_c^s , such that growth halts for $J^s < J_c^s$. The swelling ratio in the absence of any constraints has a preferred value (established in the next section) and it can fall due to applied stresses and diffusion-consumption effects. If it falls to or below the critical swelling ratio, growth halts, and thus it is a critical parameter in capturing the effects of mechanical and diffusion-consumption constraints on growth. From Figure 3, it can be seen that the critical swelling ratio J_c^s depends on both χ and η . The critical solid volume fraction $\phi_c = 1/J_c^s$ can be defined as the maximum value of the solid volume fraction above which growth ceases and has been plotted in Figure 4(b) as a function of χ for different values of η . For a fixed value of χ , increasing values of η lead to lower values of ϕ_c , or equivalently higher values of J_c^s . At a given value of $\Delta\bar{\mu}_0$, increasing values of χ lead to smaller values⁸ of J_c^s . In the limit $\eta \rightarrow -\infty$, that is the conversion energy being extremely favourable for growth, $\phi_c \rightarrow 1$, which means that the solid would have to be completely dry to stop growing and even a small amount of swelling would lead to growth. In the limit $\eta \rightarrow 1$, it can be shown that $\phi_c = 1/J_{\text{max}}^s$.

5.2. Uniform growth without diffusion-consumption limitations ($\tau_g/\tau_d \rightarrow \infty$)

We have shown in the previous section that the growth in systems with small G/μ^* is primarily dependent on the swelling ratio and thus, to study the effect of applied stresses and diffusion-consumption limitations on growth, we would have to study their effect on the swelling ratio. Accounting for diffusion-consumption effects requires a full spatial solution of the coupled governing equations in Section 3.7, which follows in later sections. Here we isolate the effects of mechanical constraints on growth by considering uniform swelling-growth that emerges in the infinitely fast diffusion limit ($\tau_g/\tau_d \rightarrow \infty$) for the case of uniform applied pressure and chemical potential on the boundary. The results from this section also aid analysis in later sections where

⁸The dependence of ϕ_c on χ for a fixed η can be non-monotonic as seen in Figure 4(b) since $\Delta\bar{\mu}_0^c$ is a function of χ and thus a fixed value of η does not necessarily correspond to a fixed value of $\Delta\bar{\mu}_0$ for varying χ .

we include diffusion-consumption limitations.

Setting $\tau_g/\tau_d \rightarrow \infty$, the equilibrated diffusion-consumption equation (82) reduces to

$$\overline{\text{Div}}(\overline{\mathbf{M}}_{\text{mob}}\overline{\nabla}\mu) = 0 \quad (86)$$

Consider a boundary value problem where the chemical boundary condition is purely in terms of an applied chemical potential of value μ_0^f (which corresponds to a bath of diffusing species maintained at its reference chemical potential) so that $\partial\mathcal{B}_j^R = \emptyset$, $\partial\mathcal{B}_\mu^R = \partial\mathcal{B}^R$, and $\check{\mu} = \mu_0^f$ in eqs. (54) and (55). Additionally, assume that the mechanical boundary condition is purely in terms of an applied Cauchy pressure of value P_b so that $\partial\mathcal{B}_x^R = \emptyset$, $\partial\mathcal{B}_t^R = \partial\mathcal{B}^R$, and $\check{\mathbf{s}} = -JP_b\mathbf{F}^{-T}\mathbf{n}_R$ in eqs. (52) and (53). It can be shown that the solution fields for the deformation tensors and the stresses are spatially uniform and spherical and that the chemical potential is spatially uniform, such that

$$\mathbf{F}^s = (J^s)^{\frac{1}{3}}\mathbf{I} = \phi^{-\frac{1}{3}}\mathbf{I}, \quad \mathbf{F}^g = (J^g)^{\frac{1}{3}}\mathbf{I}, \quad \mathbf{F}^e = (J^e)^{\frac{1}{3}}\mathbf{I}, \quad \mathbf{T} = -P_b\mathbf{I}, \quad \mu = \mu_0^f \quad (87)$$

Using eqs. (58), (62) and (87), the uniform elastic and swelling deformations can be obtained as the solution to the following coupled set of equations,

$$\mu^{\text{mix}}(\phi) - K \ln(J^e)\phi = 0 \quad (88)$$

$$G \left((J^e)^{\frac{2}{3}}\phi^{\frac{1}{3}} - \phi \right) + \mu^{\text{mix}}(\phi) + J^e P_b = 0 \quad (89)$$

where $\mu^{\text{mix}}(\phi)$ is defined in eq. (61). If we further restrict ourselves to the limit of perfect incompressibility so that $K/G \rightarrow \infty$, then $J^e \rightarrow 1$, and the two equations reduce to one equation that relates the applied pressure and the swelling ratio (Appendix B.1),

$$\left(\phi^{\frac{1}{3}} - \phi \right) + \left(\frac{\mu^*}{G} \right) \bar{\mu}^{\text{mix}}(\phi) + \bar{P}_b = 0 \quad \text{where} \quad \bar{P}_b = \frac{P_b}{G} \quad (90)$$

The solution for ϕ in eq. (90) is the equilibrium solid volume fraction as a function of the applied pressure in the limit of infinitely fast diffusion and perfect incompressibility, which we denote by $\phi_{eq}(\bar{P}_b)$. The related swelling ratio is given by $J_{eq}^s(\bar{P}_b) = 1/\phi_{eq}$.

To solve for the swelling in eq. (90), we cannot set $G/\mu^* \rightarrow 0$ as this leads to $\phi_{eq} \rightarrow 0$ (infinite swelling) for $\chi < 0.5$. Thus here we set $G/\mu^* = 4 \times 10^{-5}$, which is a representative value for tumors and bacterial biofilm systems that we model later. The equilibrium solid volume fraction ϕ_{eq} is plotted as a function of the dimensionless applied pressure \bar{P}_b in Figure 5(a) for various values of χ . We only plot positive values of pressure, as a solution for ϕ_{eq} is not necessarily guaranteed for negative pressures $\bar{P}_b < 0$ (diffusion equilibrium might not be possible). It can be seen that the larger the applied pressure, the higher the equilibrium solid volume fraction or consequently the lower the equilibrium swelling ratio as one would intuitively expect. Given that we know from the previous section that the growth rate generally decreases with decreasing swelling ratio, this

explains why the growth rate decreases in the presence of mechanical confinement⁹. For a given value of applied pressure it can be seen that higher values of χ , which corresponds to greater dis-affinity between the solid and diffusing species, leads to higher solid volume fraction or lower swelling ratio. Finally, we define the free solid volume fraction ϕ_f and the free swelling ratio J_f^s as follows

$$\phi_f = \phi_{eq}(\bar{P}_b = 0), \quad J_f^s = 1/\phi_f \quad (91)$$

which characterize the swelling state under free-growth conditions in the absence of stresses and diffusion-consumption constraints.

The dimensionless driving stress for volumetric growth, \bar{f}_g , specializes for uniform isotropic growth in the limit of infinitely fast diffusion and perfect incompressibility as follows (Appendix B.1)

$$\bar{f}_g = \bar{f}_g^\infty = \Delta\bar{\mu}_0 + \bar{f}_g^{\text{mix}}(\phi) + \frac{G}{\mu^*} \left(\ln(\phi^{-1}) - \frac{1}{2} \left(\phi^{-\frac{2}{3}} - 1 \right) \right) \quad (92)$$

wherein the driving stress remains a function of the swelling and there is one additional term compared to eq. (83) to account for the finite value of G/μ^* . Note that for the small value of G/μ^* considered here, \bar{f}_g , the critical solid volume fraction ϕ_c , and the dimensionless critical conversion energy $\Delta\bar{\mu}_0^c$, are practically unchanged from their values at the limit $G/\mu^* \rightarrow 0$ from the previous section. Nevertheless, we solve for the exact values of $\Delta\bar{\mu}_0^c$ and ϕ_c using the following equations,

$$\Delta\bar{\mu}_0^c = - \max_{0 \leq \phi \leq 1} (\bar{f}_g^\infty - \Delta\bar{\mu}_0), \quad \bar{f}_g^\infty(\phi_c) = 0 \quad (93)$$

We can define a homeostatic pressure P_h as the applied pressure that results in an equilibrium solid volume fraction equal to the critical value that stops growth, so that

$$\phi_{eq}(\bar{P}_h) = \phi_c \quad \text{where} \quad \bar{P}_h = \frac{P_h}{G} \quad (94)$$

The homeostatic pressure is the preferred pressure state that the system tends to and stops growing at, for the case of uniform applied pressure in absence of diffusion-consumption limitations. Using eq. (87), the related homeostatic stress state is given by $\mathbf{T}_h = -P_h \mathbf{I}$. The dimensionless homeostatic pressure is plotted as function of the conversion energy ratio η in Figure 5(b). The more favourable the conversion energy (smaller η) or smaller the value of χ , the larger the homeostatic pressure. Further, the ratio $\phi_f/\phi_c = J_c^s/J_f^s$ is plotted in Figure 5(c), the homeostatic pressure is positive when it is smaller than one (since J_f^s is the swelling at zero pressure and the swelling ratio decreases monotonically with increasing applied pressure) while the homeostatic pressure is negative when it is larger than one. Hence, the homeostatic pressure is mostly positive except for small negative values at high values of χ and η . Thus for the uniform swelling-growth problem considered here, *our swelling-growth theory offers a kinetic basis for the typically phenomenologically prescribed homeostatic stress, its relation to underlying material parameters, and for why it is typically observed to be compressive for soft growing systems*. However, note that for a general boundary value problem, there is no fixed stress state (dependent on material parame-

⁹It was numerically verified that $J_{eq}^s(\bar{P}_b \geq 0) \leq J_{\text{max}}^s$ irrespective of χ and thus the growth rate necessarily decreases with increasing positive pressure (\bar{f}_g increases monotonically with J^s for $J^s < J_{\text{max}}^s$).

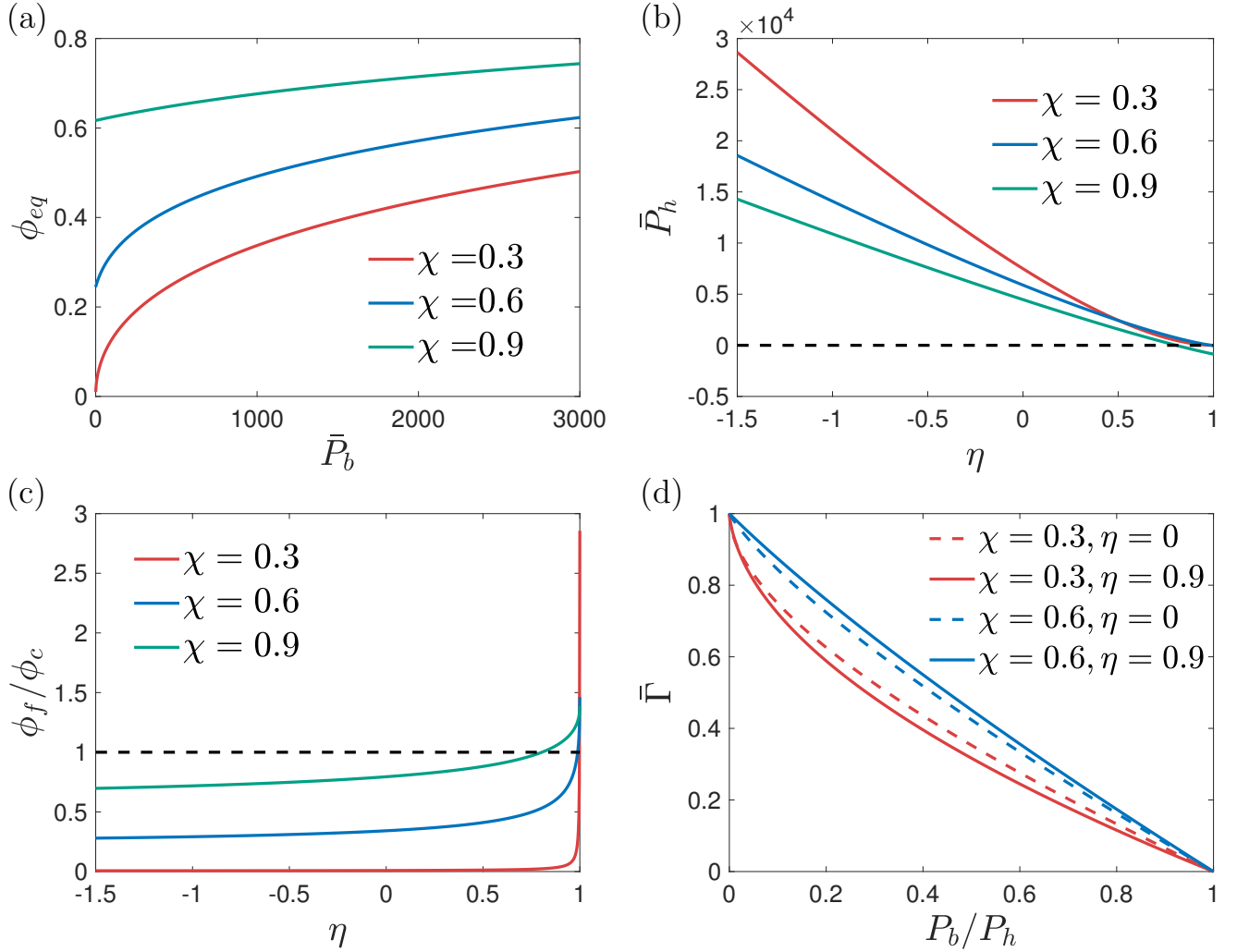


Figure 5: Uniform swelling-growth that emerges for uniform applied pressure P_b and infinitely fast diffusion ($\tau_g/\tau_d \rightarrow \infty$), in the limit of perfect incompressibility. Plots, for various χ , of (a) The equilibrium value of solid volume fraction, ϕ_{eq} , as a function of dimensionless applied pressure \bar{P}_b . (b) The dimensionless homeostatic pressure (\bar{P}_h) as a function of the conversion energy ratio (η). (c) The ratio of the free solid volume fraction (ϕ_f) to the critical solid volume fraction (ϕ_c), as a function of the conversion energy ratio. (d) Plots, for various χ and η , of the dimensionless volumetric growth rate as a function of P_b/P_h , the ratio of applied pressure to the homeostatic pressure.

ters alone) that stops growth based on our growth laws. This emphasizes the need to move away from phenomenological prescriptions as experimental observations under specific conditions need not translate to other scenarios.

Finally, we show the dependence of the dimensionless growth rate as a function of the applied pressure using eqs. (75), (90) and (92). The growth rate only depends on the solid volume fraction which only depends on the applied pressure here in the absence of diffusion-consumption limitations. We choose $\bar{f}_g^* = \bar{f}_g(\phi_f)$ so that $\bar{\Gamma} = 1$ when $P_b = 0$. The dimensionless growth rate $\bar{\Gamma}$ is plotted as a function of P_b/P_h in Figure 5(d) for different values of χ and η ($P_h > 0$ for all combinations of chosen χ and η). It can be seen that larger applied pressure (higher values

of P_b/P_h) always leads to decreasing growth rates. For $P_b/P_h > 1$, we have $\bar{\Gamma} = 0$. Hence, our swelling-growth theory also offers a kinetic basis for the experimentally observed dependence of growth rate on applied stresses.

We note that all the conclusions above also hold for the case of non-isochoric species conversion (see Appendix A.4). Having demonstrated the ability of the theory to qualitatively capture the different experimentally observed dependences of the growth rate on the concentration of the diffusing species and the applied stress (in the absence of diffusion-consumption effects), we will now employ the theory to solve boundary value problems where these dependences become relevant.

5.2.1. Growth under mechanical confinement without diffusion-consumption limitations

First, we consider the problem of growth under mechanical confinement in the limit of perfect incompressibility and infinitely fast diffusion so that we neglect diffusion-consumption limitations. The results will already demonstrate the coupling between swelling and growth and how the notion of homeostatic stress developed in the previous section manifests in a physical boundary value problem.

We consider mechanical confinement in the form of a deformable spherical shell and assume the growing body is spherical, so that $\partial\mathcal{B}^R$ is the surface of a sphere. The confining shell is taken to have inner and outer radial dimensions, A and B respectively, so that B/A is a thickness measure of the shell. It is assumed to be non-growing ($\mathbf{F}^g = \mathbf{I}$), non-swelling ($\mathbf{F}^s = \mathbf{I}$), perfectly incompressible ($J^e \rightarrow 1$) and made up of a strain stiffening material described by a Mooney-Rivlin model (Mooney, 1940; Rivlin, 1948) so that its reference free energy ψ_R is of the form (Boulanger and Hayes, 2001)

$$\psi_R = \frac{G_c}{2} ((1-n)(\text{tr}(\mathbf{B}) - 3) + n(I_2(\mathbf{B}) - 3)), \quad I_2(\mathbf{B}) = \frac{1}{2} ((\text{tr}(\mathbf{B}))^2 - \text{tr}(\mathbf{B}^2)) \quad (95)$$

where G_c is the linear shear modulus of the confinement, n is a stiffening parameter (larger the n the more the stiffening) and $\mathbf{B} = \mathbf{B}^e$. It can be shown (Chen, 2018) that the pressure applied by the mechanical confinement upon deformation only depends on the circumferential stretch of its inner boundary, λ_a , so that

$$\frac{P_b}{G_c} = \frac{1-n}{2} (4\lambda_b^{-1} + \lambda_b^{-4} - \lambda_a^{-4} - 4\lambda_a^{-1}) + \frac{n}{2} (-4\lambda_b + 2\lambda_b^{-2} + 4\lambda_a - 2\lambda_a^{-2}) \quad (96)$$

where the circumferential stretch at the outer boundary, λ_b , is expressed in terms of λ_a due to incompressibility by the relation

$$\lambda_b = \left(1 + (\lambda_a^3 - 1) \left(\frac{A}{B} \right)^3 \right)^{\frac{1}{3}} \quad (97)$$

We assume that, at $t = 0$, the undeformed inner boundary of the shell is just in contact with the initially diffusion equilibrated growing body, so that the circumferential stretch of the confining shell is $\lambda_a^3 = J/J_0$, where J is the volume ratio of the uniformly growing body and

$J_0 = J(t = 0) = J_f^s$ is its initial value. The chemical boundary condition is still taken as $\mu = \mu_0^f$ on $\partial\mathcal{B}^R$.

We choose the following representative parameters based on our modelling of growing tumors later in Section 5.6,

$$G/\mu^* = 4 \times 10^{-5}, \quad \chi = 0.55, \quad \eta = 0.95, \quad n = 0.9 \quad (98)$$

The choice of $n = 0.9$ corresponds to a strain stiffening confinement where the pressure applied by the confinement increases continuously with deformation. Later, when we model growing bacterial biofilms in Section 5.7, we will consider neo-Hookean confinement ($n = 0$) wherein the applied pressure attains a maximum value with increasing deformation.

The form of the solution from the previous section in eq. (87) continues to apply here. To solve the boundary value problem, we need to integrate the growth evolution equation (75) (with \bar{f}_g in eq. (92)) while satisfying eqs. (90) and (96). This is done numerically and the results are plotted in Figure 6 as a function of \bar{t}_g for different cases of stiffness ratio G_c/G and confinement dimension ratio B/A . Note that the dimensionless results here are independent of dimensional parameters such as the growth constant k_g . In Figure 6(a1-a3), the results are plotted for the case of a confining medium ($B/A \rightarrow \infty$) with varying stiffness ratio G_c/G to show the effect of confining stiffness on growth (later we model bacterial biofilm growth against a confining medium). It can be seen that in the case of free growth ($G_c/G \rightarrow 0$), the swelling ratio remains unchanged during growth at its free value J_f^s . This leads to constant growth rate of $\bar{\Gamma} = 1$, i.e a straight line in log-log plot of J^g vs \bar{t}_g with slope of unity (remember that \bar{f}_g^* was chosen such that the dimensionless growth rate is unity for free growth). When the confining stiffness is finite, the applied pressure increases with deformation of the medium due to growth of the body which reduces the swelling ratio J^s (Figure 6(a2)), thus the swelling is coupled to the growth. This decrease in J^s leads to decrease in the growth rate (Figure 6(a3)) from its free growth value (growth is coupled to the swelling). The combined reduction of growth rate and J^s with time from their free growth values leads to a suppressed profile for the evolution of J/J_0 compared to free growth (Figure 6(a1)) which will be the physically observed evolution of volume of the growing body in experiments.

If the confining medium deforms enough that the applied pressure reaches the homeostatic value P_h (or equivalently the swelling ratio reaches the critical value J_c^s) discussed in the previous section, the growth will stop and the field variables stop evolving with time. The volume ratio J/J_0 at which growth will stop can be analytically evaluated by setting $P_b = P_h$ and $\lambda_a^3 = J/J_0$ in eq. (96) where P_h is solved using eq. (94). These values are plotted using dashed lines in Figure 6(a1) and are confirmed to match with simulations. As one would intuitively expect, larger confining stiffness lowers the growth rate and leads to smaller steady size of the growing body since the homeostatic stress (or critical swelling ratio) is reached at smaller deformations (Figure 6(a1)). Such behaviour has been observed in tumors growing against a confining medium (Helmlinger et al., 1997). Note that, for a neo-Hookean confinement (i.e non stiffening so that $n = 0$), the applied pressure will saturate at a maximum cavitation pressure with increasing deformation. If the homeostatic pressure is larger than this cavitation pressure, the body will

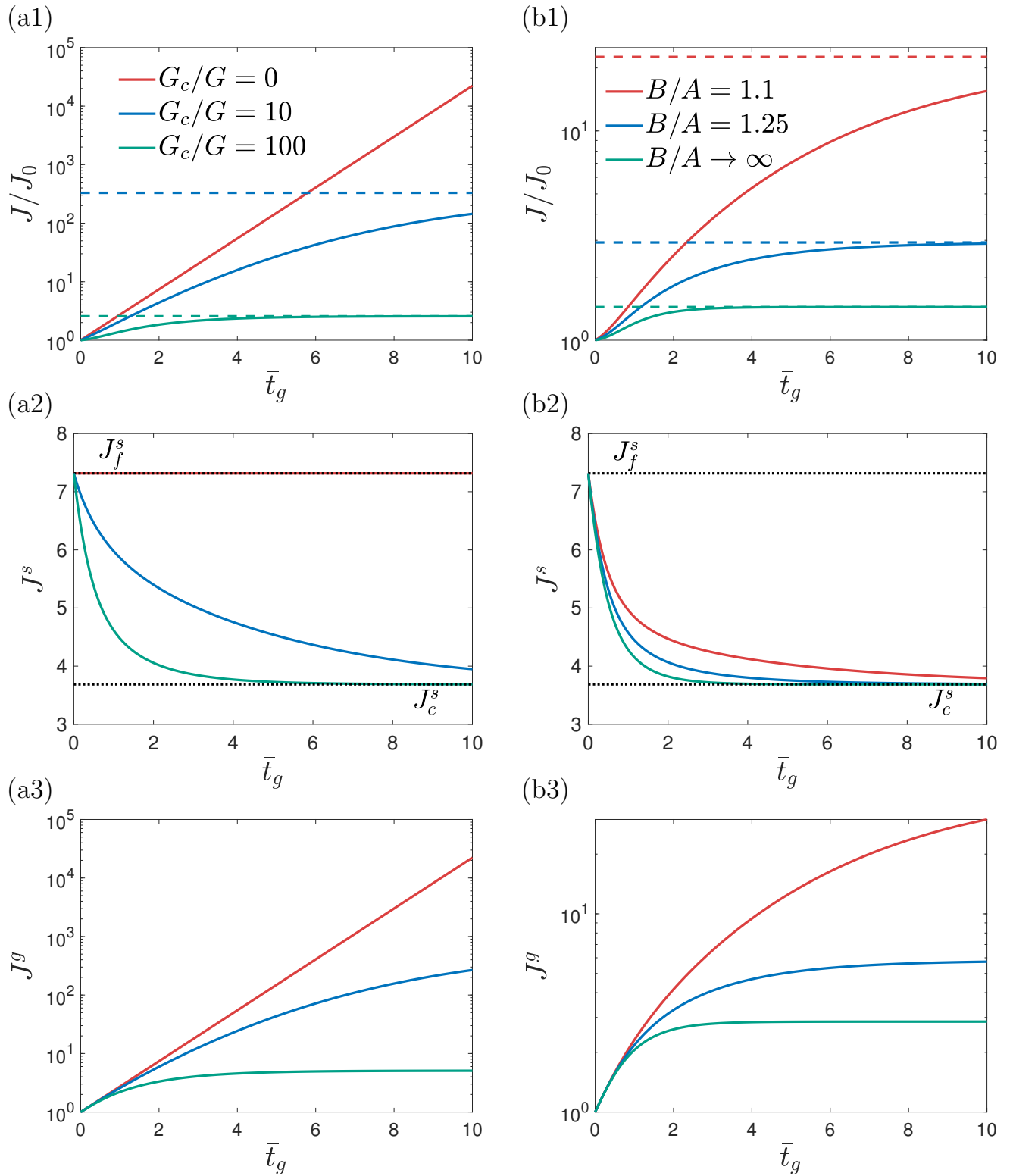


Figure 6: Temporal evolution of variables for uniform swelling-growth against mechanical confinement, in the limit of infinitely fast diffusion ($\tau_g/\tau_d \rightarrow \infty$) and perfect incompressibility, with $n = 0.9$. (a1-a3) Plots for a confining medium ($B/A \rightarrow \infty$) for varying modulus ratio of confinement to the growing body (G_c/G). (b1-b3) Plots for confining shells with varying dimension ratio B/A (outer to inner dimension) and fixed modulus ratio $G_c/G = 250$. The dashed lines in (a1) and (b1) correspond to the analytic homeostatic limit.

never stop growing due to the confinement. We will see such behavior in the bacterial biofilm growth experiments we model later.

Next, we demonstrate the effect of varying thickness of the spherical shells for a fixed value of $G_c/G = 250$ in Figure 6(b1-b3). The same discussion above for the case of varying stiffness ratio applies again and it can be seen that larger thicknesses of the confinement for a given stiffness ratio lead to smaller steady sizes as one would intuitively expect and as seen in the tumor experiments in Section 2. The assumption of infinitely fast diffusion employed so far prevents accounting for diffusion-consumption effects which are important for large volumetric growth. We relax this assumption in the following sections.

5.3. Spherically symmetric equations

To account for diffusion-consumption effects as the body is growing, we need to account for spatially varying field variables. We restrict the analysis to a spherically symmetric setting and consider a swelling and growing body subjected to a uniform external pressure and immersed in a bath of diffusing species maintained at a constant reference chemical potential. The dry reference body is described by the radial coordinate $R \in [0, R_0]$ and the current radial coordinates is given by $r = r(R)$ where $r(0) = 0$ and $r(R_0)$ is the current radius of the body. Choosing $L^* = R_0$ to non-dimensionalize the problem, we have dimensionless reference coordinates $\bar{R}(= R/R_0) \in [0, 1]$ and dimensionless current coordinates $\bar{r} = r/R_0 = \bar{r}(\bar{R})$. The deformation gradient in spherical basis and associated volume ratio J can then be written as

$$\mathbf{F} = \text{diag} [\lambda_r, \lambda_\theta, \lambda_\theta] = \text{diag} \left[\frac{\partial \bar{r}}{\partial \bar{R}}, \frac{\bar{r}}{\bar{R}}, \frac{\bar{r}}{\bar{R}} \right], \quad J = \lambda_r \lambda_\theta^2 \quad (99)$$

where λ_r is the radial stretch and λ_θ is the circumferential stretch. The elastic, swelling, and elasto-swelling deformation gradient tensors $\mathbf{F}^e, \mathbf{F}^s, \mathbf{F}^{es}$, and their associated determinants can be written as

$$\mathbf{F}^i = \text{diag} [\lambda_r^i, \lambda_\theta^i, \lambda_\theta^i], \quad J^i = \lambda_r^i \lambda_\theta^{i2} \text{ for } i = \{g, e, es\} \quad (100)$$

where the different stretches are related as follows

$$\lambda_i^e = \frac{\lambda_i}{\lambda^s \lambda_i^g}, \quad \lambda_i^{es} = \frac{\lambda_i}{\lambda_i^g}, \quad \text{for } i = \{r, \theta\} \quad (101)$$

Thus, given $\bar{r}(\bar{R})$, λ_r^g , λ_θ^g , and λ^s , all deformation gradient tensors can be determined. The dimensionless Cauchy and Piola stresses in eqs. (72) and (73) specialize as

$$\bar{\mathbf{T}} = \text{diag} [\bar{T}_r, \bar{T}_\theta, \bar{T}_\theta], \quad \bar{T}_i = \frac{1}{J^{es}} \left((\lambda_i^{es2} - 1) + \frac{K}{G} \ln(J^e) \right) \text{ for } i = \{r, \theta\}, \quad (102)$$

$$\text{and } \bar{\mathbf{S}} = \text{diag} [\bar{S}_R, \bar{S}_\Theta, \bar{S}_\Theta], \quad \bar{S}_R = \lambda_\theta^2 \bar{T}_r, \quad \bar{S}_\Theta = \lambda_r \lambda_\theta \bar{T}_\theta \quad (103)$$

respectively. The dimensionless mechanical equilibrium equation (73) under spherical symmetry is given by

$$\frac{d\bar{S}_R}{d\bar{R}} + \frac{2}{\bar{R}} (\bar{S}_R - \bar{S}_\Theta) = 0 \quad (104)$$

The equilibrated diffusion-consumption equation eq. (86) meanwhile specializes as

$$J^s J^g \bar{\Gamma} \left(\frac{\tau_d}{\tau_g} \right) = \frac{1}{\bar{R}^2} \frac{\partial (\bar{R}^2 \bar{M}_{\text{mob}}^R \frac{\partial \bar{\mu}}{\partial \bar{R}})}{\partial \bar{R}} \quad \text{where} \quad \bar{M}_{\text{mob}}^R = \frac{\lambda_\theta^2}{\lambda_r} \quad (105)$$

, the dimensionless chemical potential $\bar{\mu}$ is defined in eq. (71), and the dimensionless mobility tensor is specialized from eq. (70)₂.

The volumetric growth evolution is given by eq. (75) where \bar{f}_g specializes as

$$\bar{f}_g = \Delta \bar{\mu}_0 + \bar{f}_g^{\text{mix}}(\phi) + \frac{G}{\mu^*} \left(\ln(J^{es}) - \frac{K}{2G} (\ln(J^e))^2 - \frac{1}{6} (\lambda_r^{es2} + 2\lambda_\theta^{es2} - 3) \right) \quad (106)$$

We choose $\bar{f}_g^* = \bar{f}_g^\infty(\phi_f)$ for normalizing the growth law, where \bar{f}_g^∞ is defined in eq. (92) and ϕ_f is the free solid volume fraction for free growth in the limit of infinitely fast diffusion and perfect incompressibility, given by eq. (91). The growth directionality evolution equation eq. (79) specialize for spherical symmetry as follows

$$\frac{1}{\lambda_r^g} \frac{d\lambda_r^g}{dt_g} = \frac{\bar{\Gamma}}{3} - \frac{2G}{9\mu^* \bar{f}_g^*} (\lambda_\theta^{es2} - \lambda_r^{es2}), \quad \frac{1}{\lambda_\theta^g} \frac{d\lambda_\theta^g}{dt_g} = \frac{\bar{\Gamma}}{3} + \frac{G}{9\mu^* \bar{f}_g^*} (\lambda_\theta^{es2} - \lambda_r^{es2}) \quad (107)$$

where $\bar{\Gamma}$ is given by eq. (75). It can be shown that only two of the three evolution equations in eqs. (75) and (107) are independent and therefore we have two independent evolution equations for the growth (since essentially prescription of two of the three among λ_r^g , λ_θ^g , and J^g automatically determines the third through eq. (100)₂). We thus have four field variables (\bar{r} , λ_r^g , λ_θ^g , and λ^s) and four governing equations (eqs. (104), (105) and (107)). The prescription of boundary conditions for eqs. (104) and (105), and initial conditions for equations in (107) complete the definition of a solvable boundary value problem.

For the initial conditions for growth evolution, we set $\mathbf{F}_g^0 = \mathbf{I}$ which reduces to the following choices for spherical symmetry

$$\lambda_r^g(\bar{R}, t = 0) = 1, \quad \lambda_\theta^g(\bar{R}, t = 0) = 1 \quad (108)$$

The following boundary conditions are prescribed for the radial stress and chemical potential at the outer boundary

$$\bar{T}_r(\bar{R} = 1, t) = -\bar{P}_b(t), \quad \bar{\mu}(\bar{R} = 1, t) = \bar{\mu}_0^f \quad (109)$$

where $\bar{P}_b(t)$ is the applied dimensionless pressure, related to the applied pressure $P_b(t)$ through the relation $\bar{P}_b(t) = P_b(t)/G$.

The spherically symmetric equations are solved using a numerical scheme outlined in Appendix C. For solving the equations in dimensionless space, the only material parameters of the growing body that need to be specified are χ , $\Delta \bar{\mu}_0$, τ_g/τ_d , G/μ^* , and K/G . Note from eqs. (71), (105) and (109) that the value of $\bar{\mu}_0^f$ does not affect any of the solution field variables of the problem except to shift the chemical potential by a constant value. Thus without loss of generality we

set $\bar{\mu}_0^f = 0$. The parameter $\Delta\bar{\mu}_0$ can be replaced with the conversion energy ratio $\eta = \Delta\bar{\mu}_0/\Delta\bar{\mu}_0^c$ where $\Delta\bar{\mu}_0^c$ is evaluated using eq. (93)₁.

Since the fields now spatially vary, we define the following volume averaged parameters,

$$\bar{J} = 3 \int_0^1 J \bar{R}^2 d\bar{R}, \quad \bar{J}^s = 3 \int_0^1 J^s \bar{R}^2 d\bar{R}, \quad \bar{J}^g = 3 \int_0^1 J^g \bar{R}^2 d\bar{R}, \quad \bar{J}_0 = \bar{J}(t=0) \quad (110)$$

where \bar{J} is the total volume ratio of the body with respect to its dry reference volume, \bar{J}_0 is initial value of \bar{J} and \bar{J}/\bar{J}_0 is the total volume ratio of the body compared to its initial equilibrium volume (Note that we are solving the diffusion equilibrated version of the governing equations so that $\bar{J}_0 \neq 1$). It can be shown using eqs. (99) and (110)₁ that $\bar{J} = \bar{r}^3(\bar{R} = 1) = \lambda_g^3(\bar{R} = 1)$.

In Section 5.4 we consider free growth so that $\bar{P}_b = 0$ and in Section 5.5 we consider a constant applied pressure $\bar{P}_b(t) = \bar{P}_b$. For modelling the tumor experiments in Section 5.6 and the bacterial biofilm experiments in Section 5.7, the applied pressure is described as a function of the confinement deformation using eq. (96) where $\bar{P}_b = (P_b/G_c) \times (G_c/G)$. The circumferential stretch at the inner boundary of the confining shell is now given by the following equation

$$\lambda_a^3 = \begin{cases} \bar{J}/J_c, & \text{if } \bar{J}/J_c \geq 1 \\ 1, & \text{if } \bar{J}/J_c < 1 \end{cases} \quad (111)$$

where J_c is the ratio of inner volume of undeformed confinement to the initial dry reference volume of the body. The conditional cases in eq. (111) reflect the fact that the confinement only starts deforming once the growing body comes in contact with it.

5.4. Free growth with diffusion-consumption limitations

In this section, we analyze the problem of free growth in the presence of diffusion-consumption limitations. We solve the spherically symmetric equations and set $P_b = 0$. Once again we consider $\chi = 0.55$ and $G/\mu^* = 4 \times 10^{-5}$. Near incompressibility is enforced by setting a high value of $K/G = 10^6$. We consider different values of the conversion energy ratio η and the growth to diffusion timescale ratio τ_g/τ_d .

The time evolution of spatially averaged variables defined in eq. (110) is plotted in Figure 7 for varying values of τ_g/τ_d at fixed conversion energy ratio η . The plots in Figure 7(a1-a3) are for the case of $\eta = 0$ and those in Figure 7(b1-b3) are for the case of $\eta = 0.9$. The dashed lines correspond to the case of infinitely fast diffusion ($\tau_g/\tau_d \rightarrow \infty$) and perfect incompressibility ($K/G \rightarrow \infty$) wherein the swelling ratio is the free value J_f^s at all times and the dimensionless growth rate is unity. The spatial profiles of the field variables are plotted at increasing times in Figure 8 for a representative case of $\eta = 0.9, \tau_g/\tau_d = 1000$ (the timescale ratio used for tumor growth modelling later).

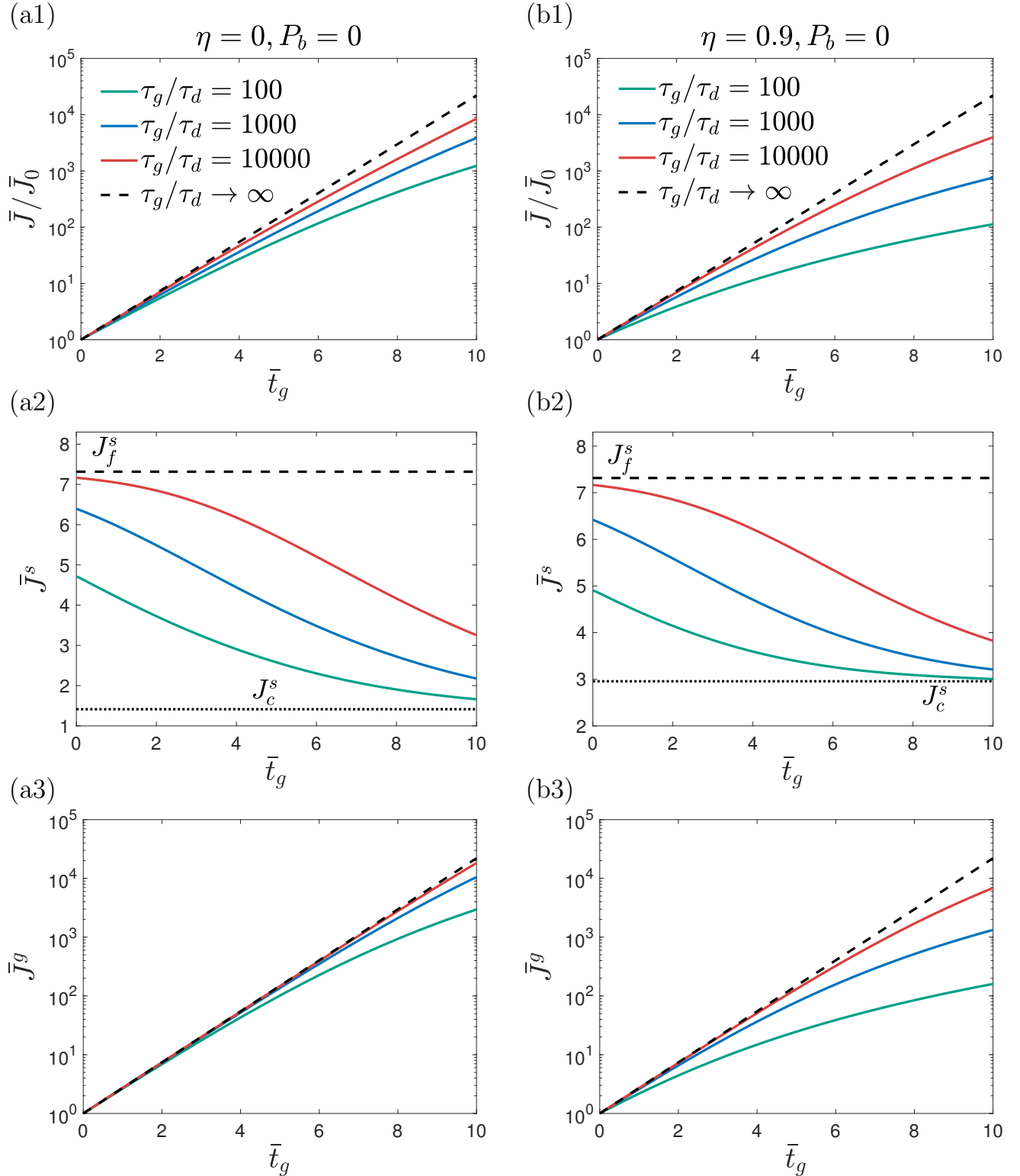


Figure 7: Plots of temporal evolution of spatially averaged quantities for the case of free growth with diffusion-consumption limitations, for various values of τ_g/τ_d . (a1-a3) Plots for the case of zero species conversion energy. (b1-b3) Plots for the case of conversion energy ratio $\eta = 0.9$. The dashed lines correspond to the limit of infinitely fast diffusion ($\tau_g/\tau_d \rightarrow \infty$) and perfect incompressibility ($K/G \rightarrow \infty$).

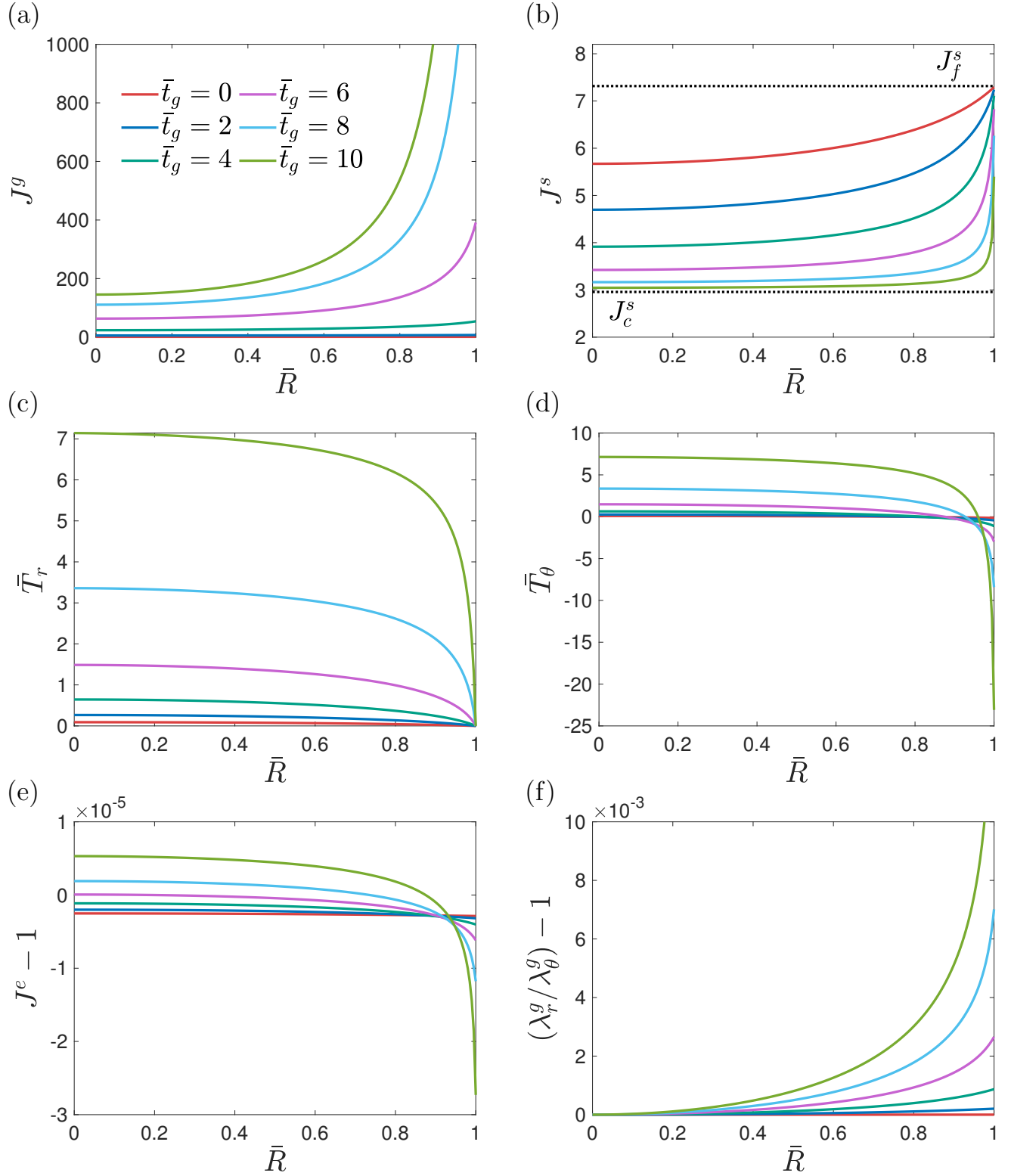


Figure 8: Plots of spatial variation of solution fields (over dimensionless referential radial coordinate \bar{R}) for free growth with diffusion-consumption limitations, at various times, for representative case of $\eta = 0.9, \tau_g/\tau_d = 1000$.

When τ_g/τ_d is finite, it is seen from Figure 8(b) that the equilibrium swelling ratio profile is spatially decreasing from the outer edge of the growing body to the inside, due to diffusion-consumption balance, and that this profile drops with time as the body swells and grows. This leads to spatially decreasing volumetric growth rates from the outside to inside which all drop with time. Consequently the spatially averaged swelling ratio (\bar{J}^s) drops with time (Figure 7(a2,b2)), as does the spatially averaged growth rate as seen by the decreasing slope with time of the log-log plot of \bar{J}^g vs \bar{t}_g in Figure 7(a3,b3). The combined drop in swelling ratio and growth rates lead to decreasing overall volume increase rate, resulting in a decreasing slope with time of the log-log plot of \bar{J}/\bar{J}_0 vs \bar{t}_g in Figure 7(a1,b1). For a given η , smaller values of τ_g/τ_d result in lower swelling ratio profiles at all times as can be seen by comparing Figure 9(a) where the spatial profiles of the swelling ratio are plotted for the case of $\eta = 0.9, \tau_g/\tau_d = 100$ with the curves in Figure 8(b) for $\eta = 0.9, \tau_g/\tau_d = 1000$ (due to a smaller consumption term on the left hand side of eq. (105)). Consequently for a given η , smaller values of τ_g/τ_d lead to larger decrease with time in spatially averaged swelling ratio, growth rates, and volume increase rate, as seen in Figure 7. Further, for increasing τ_g/τ_d , the curves correctly approach the results for infinitely fast diffusion limit ($\tau_g/\tau_d \rightarrow \infty$). Thus, the presence of diffusion-consumption effects leads to decreased growth and volume increase rates both with time and in comparison to the constant free growth rate in the infinitely fast diffusion limit. Finally, we note that the higher the conversion energy ratio η for a given τ_g/τ_d , the more pronounced the drop in averaged growth rate and volume increase rate compared to their values in the corresponding infinitely fast diffusion limit¹⁰. This is due to the fact that a larger value of η corresponds to a smaller value of $\Delta\mu_0$ (when all other parameters are fixed) which can be shown to lead to a smaller dimensionless growth rate at a given swelling ratio (see Appendix A.5).

The spatial variation of the growth volume ratio J^g in Figure 8(a) at increasing times is consistent with the earlier discussion wherein the growth rates are spatially decreasing from the outer edge of the body to the inside due to the spatial variation of swelling ratio. The dimensionless radial stress profiles are plotted in Figure 8(c). The radial stress is zero on the outer boundary due to the boundary condition for free growth while being increasingly tensile towards the core of the body, with the stress variation becoming more pronounced with increasing time. This is due to the fact that the outer layers are growing at a faster rate and pulling on the slower growing inner layers. The dimensionless circumferential stress plots in Figure 8(d) indicate the circumferential stress is tensile in most of the growing body but is compressive near the outer edge. This is due to mechanical equilibrium arising from the combined effects of swelling and growth and is not intuitive, nevertheless the spatial variation in radial and circumferential stress profiles is consistent with previous studies (Ambrosi and Mollica, 2002; Xue et al., 2016). Note that the high tensile stresses in the core at large growth volumes can lead to cavitation in the growing body, see for example Goriely et al. (2010); McMahan et al. (2010). In the context of tumors and bacteria, this might manifest in the form of tendency of cells to liquefy. However, the high surface tension of the diffusing fluids at small length scales such as in tumors and bacteria could also delay such failure. Nevertheless, the ability to account for large deformations in our

¹⁰Note that the value of \bar{f}_g^* chosen to normalize the growth law is different for different η (since we enforce dimensionless volumetric growth rate of 1 for free growth with no diffusion-consumption limitations, irrespective of conversion energy).

swelling growth theory allows the possibility to access such nonlinear phenomena which might be critical to understanding growing biological systems. Next, from the plots of the elastic volume ratio in Figure 8(e), we can verify that the simulations are indeed in the nearly incompressible limit ($J^e - 1 \rightarrow 0$). The quantity $\lambda_r^g/\lambda_\theta^g - 1$ is a measure of the anisotropy of growth, the closer it is to zero the more isotropic the growth. This anisotropy measure is plotted in Figure 8(f) and the growth is seen to be nearly spherical or isotropic at all times which is consistent with the discussion in Section 4.5 due to low value of G/μ^* and our choice of growth laws. Nevertheless, the growth is seen to be more anisotropic towards the outer edge of the body and at increasing times, with the radial growth stretch being higher than the circumferential growth stretch. This is due to the fact that the circumferential stress is always more compressive (or less tensile) than the radial stress which leads to suppressed circumferential growth in comparison to the radial growth, and this stress difference is more pronounced for larger radial coordinate and at increasing times.

Revisiting the spatial swelling profiles in Figure 8(b) and Figure 9(a), we note that the swelling ratio is seen to not drop below the critical value J_c^s . When J^s approaches J_c^s the growth rate $\bar{\Gamma}$ drops to zero which results in zero consumption of the diffusing species locally (see eq. (82)), thus halting local reduction in swelling. At very large times, the vast majority of the body is seen to be at the critical swelling ratio J_c^s which means that the growth is confined to a thin outer rim. We note that the growth can technically never completely stop at the outer edge since, as discussed in Section 4.5, $\mathbf{L}^g = \mathbf{0}$ necessitates a hydrostatic stress state and this requires $\mathbf{T} = \mathbf{0}$ at the outer boundary (since $T_r = 0$). Zero stress ($\mathbf{T} = \mathbf{0}$) along with $\mu = \mu_0^f$ at the boundary would necessitate the swelling ratio at the boundary to be the free swelling ratio which is not compatible with zero growth rate. However, since G/μ^* is very small, the volumetric growth can nearly stop when the swelling ratio approaches the critical value over the entire body from accumulating stresses (the remodelling relieves stresses that can resume volumetric growth but this process is slow since G/μ^* is very small). We note that as the body grows to very large volumes, the use of the equilibrated version of the diffusion-consumption equation will become less accurate. However the accurate simultaneous integration of growth evolution equations along with non-equilibrated diffusion-consumption equation is numerically prohibitive due to the large τ_g/τ_d , strong swelling-growth coupling, and extreme growth sizes.

5.5. Growth under constant applied pressure with diffusion-consumption limitations

We now consider the combined effects of applied pressure ($P_b \neq 0$) and diffusion-consumption limitations on the growth. The same parameters from the previous section for free growth have been employed here. The applied pressure is taken to be constant so that $\bar{P}_b(t) = \bar{P}_b$. Using the value of homeostatic pressure P_h developed for the limit of infinitely fast diffusion and perfect incompressibility in Section 5.2, we consider different levels of applied pressure P_b by considering different values of the ratio P_b/P_h (which is also equal to \bar{P}_b/\bar{P}_h). The results are plotted in Figure 10 for different values of η and τ_g/τ_d . Since much of the physics is similar to the case of free growth, only the temporal evolution of \bar{J}/\bar{J}_0 is shown for sake of brevity, while a representative plot of the spatial profile evolution of J^s is shown in Figure 9(b) for the case $\eta = 0.9, \tau_g/\tau_d = 100, P_b/P_h = 0.5$. The dashed lines in Figure 10 correspond to the limit of infinitely fast diffusion and perfect incompressibility wherein the swelling ratio will be spatially and temporally constant with a value $J_{eq}^s(\bar{P}_b)$ (defined in Section 5.2), leading to constant growth

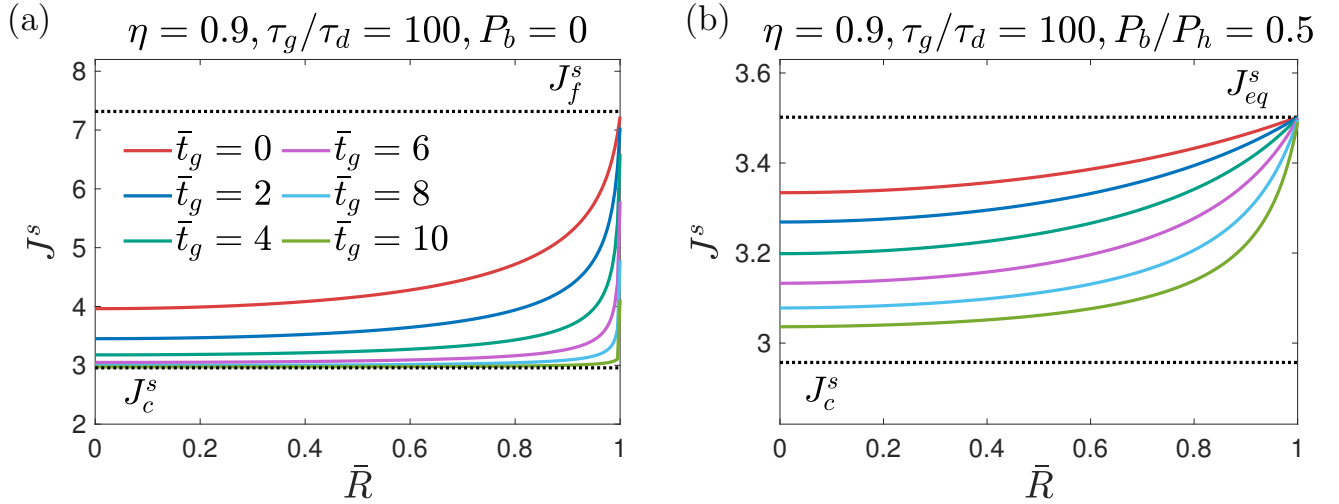


Figure 9: Plots of spatially averaged swelling ratio for growth with diffusion-consumption limitations for the case of conversion energy ratio $\eta = 0.9$ and growth to diffusion timescale ratio $\tau_g/\tau_d = 100$. (a) Free growth case (b) Case of applied pressure equal to 50% of the homeostatic pressure.

rate ($\bar{\Gamma}$ in Figure 5(d)).

Similar to the free growth case, it is seen from Figure 9(b) that as the body grows, the swelling ratio decreases everywhere. However the values of J^s are lower compared to the free growth case in Figure 9(a) due to applied pressure and the spatial profiles take longer to drop due to the reduced growth rates at smaller swelling ratios. The decreasing swelling ratio profile once again leads to decreasing volume increase rates with time in Figure 10 and the decrease is larger for smaller τ_g/τ_d when all other parameters are the same. Higher applied pressures are seen to result in reduced growth rates for a given η and τ_g/τ_d (similar to the infinitely fast diffusion limit as seen by the dashed lines). The reduction in volume increase rates compared to the infinitely fast diffusion limit is less pronounced for higher applied pressure, this is because the growth rate $\bar{\Gamma}$ is lower for higher applied pressure which results in a smaller consumption term on the left hand side of eq. (105). On the other hand, the reduction in volume increase rate compared to the infinitely fast diffusion limit is once again more pronounced for larger values of conversion energy ratio η when all other parameters are held fixed. Similar trends also apply for case of mechanical confinement considered in Section 5.2.1 when accounting for diffusion-consumption limitations, once again we skip these results for brevity and directly demonstrate application to tumor growth modelling in the next section.

5.6. Modelling tumor growth

We now model the tumor growth experiments discussed in Section 2 using our swelling-growth theory. We choose R_0 such that the initial equilibrated volume (under no applied pressure) is just in contact with the smallest confinement (Case C, inner volume = 0.003mm^3). The material parameters for the simulation are listed in Table 1 and the associated key dimensionless parameters are

$$G/\mu^* = 4 \times 10^{-5}, \quad \tau_g/\tau_d = 1000, \quad \eta = 0.972, \quad K/G = 10^6 \quad (112)$$

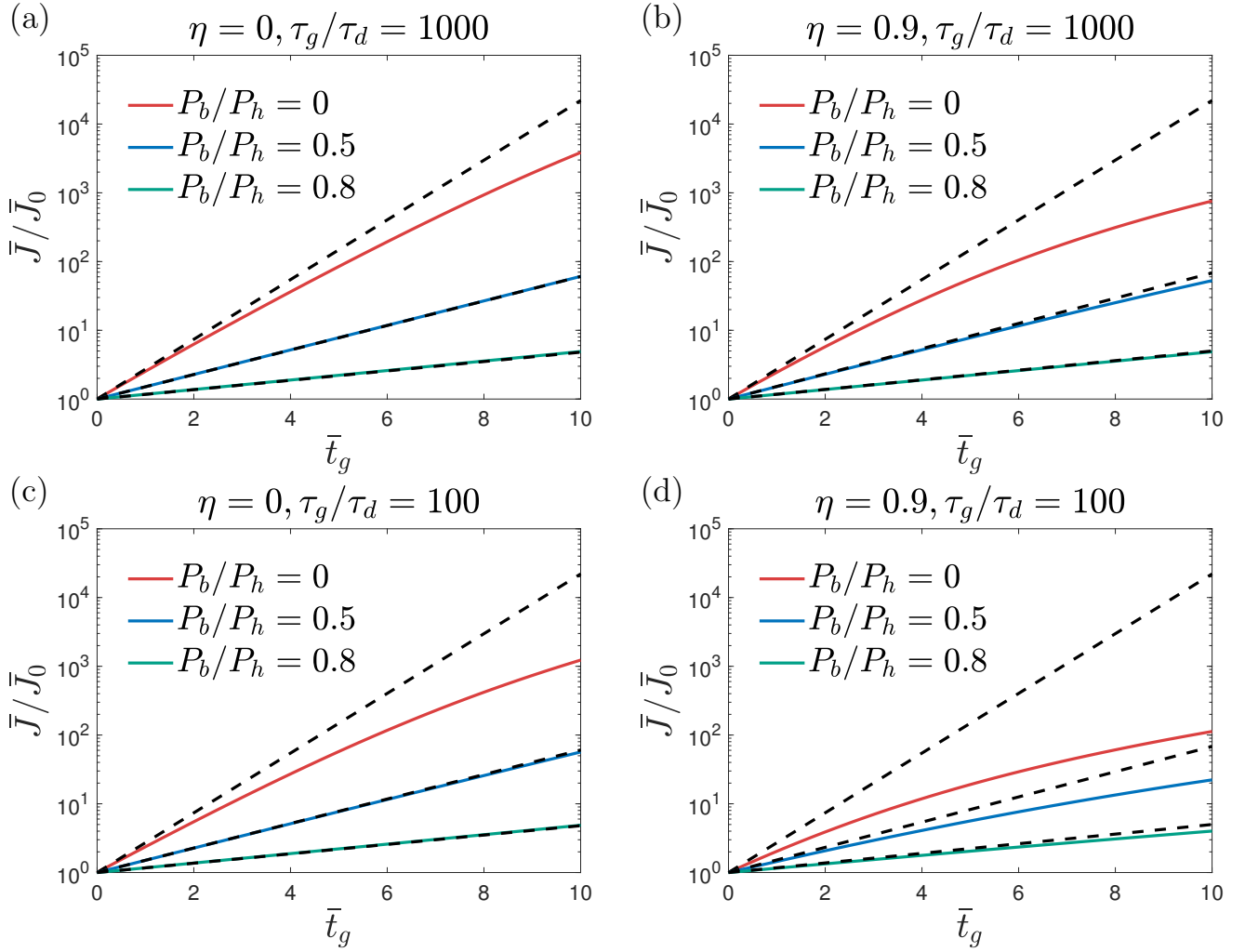


Figure 10: Plots of temporal evolution of total volume ratio with respect to initial equilibrium value (\bar{J}/\bar{J}_0) for the case of growth under uniform and constant applied pressure with diffusion-consumption limitations, for different values of conversion energy ratio η , growth to diffusion timescale ratio (τ_g/τ_d), and ratio of applied pressure to homeostatic pressure (P_b/P_h). The dashed lines represent the limit of infinitely fast diffusion ($\tau_g/\tau_d \rightarrow \infty$) and perfect incompressibility, and are shown for comparison.

We note that all parameters except the conversion energy $\Delta\mu_0$ are either obtained or directly inferred from experiments/literature or once fitted have been found to be in the range of reported values in the literature. For example, the growth timescale τ_g is directly inferred from the initial growth rate in the free growth experiments whereas the diffusion timescale τ_d is fitted for, and the resulting associated diffusion coefficient has a value $D \approx 3.6 \times 10^{-7} \text{cm}^2/\text{s}$, which is a typical value for several growth factors in tumor studies (Thorne et al., 2004; Kim et al., 2011). The dimensions of the confinement in Cases B-D are listed in Appendix C.1. For Case D, the breakage of the confinement is modelled by removing the confinement at $t = 10.35$ days. The simulated predictions of the theory are compared with the experiments in Figure 1(b), and it can be seen that the theory is able to capture all the cases well with a single set of parameters. We emphasize again the fact that unlike most conventional growth models, we have not prescribed any ad hoc functional dependence of growth evolution on concentration including critical concentration for

growth. Neither have we introduced an ad hoc homeostatic stress. The kinetic growth law based on the driving stress is automatically able to capture simultaneously the effects of both the mechanical confinement and diffusion-consumption limitations. Further, we draw attention to our relatively small parameter space compared to other tumor growth studies. Our modelling is also fully consistent, and accounts for mass balance.

Table 1: Material parameter values for modelling of tumor growth experiments

Quantity	Value	Source/Comment
R_0	56.33 μm	Chosen such that $\frac{4}{3}\pi R_0^3 \bar{J}_0 = 0.003 \text{ mm}^3$
G	1 kPa	Stylianopoulos et al. (2012)
K	1 GPa	Typical value for nearly incompressible soft polymer
τ_g	1.0317 days	Fitted from initial free growth rate
$\Delta\mu_0$	-10.15 MPa	Fitted, corresponds to $\eta = 0.972$
D	$3.6 \times 10^{-7} \text{ cm}^2/\text{s}$	Fitted, close to reported values in literature
χ	0.6	Assumed based on free tumor porosity (ϕ^f) ~ 0.25
ω^f	$1.66 \times 10^{-28} \text{ m}^3/\text{molecule}$	Hong et al. (2008)
T	300 K	Room temperature
G_c	250 kPa	Alessandri et al. (2013)
n	0.9	Fitted, confinement known to be stiffening

5.7. Modelling bacterial biofilm growth

Finally, in this section, we model experiments of swelling and growing 3D bacterial biofilms. Our collaborators at Yale University published experiments of growing 3D *Vibrio cholerae* biofilms embedded in hydrogels, as they grow by orders of magnitude from their initial size (Zhang et al., 2021). Using 3D visualization techniques with high spatio-temporal resolution, they were able to capture the growth process at the level of individual cells which allows the separate extraction of growth and swelling data. The biofilms are grown starting from a few cells to tens of thousands, against confining hydrogel medium which is replenished with nutrient filled fluid. The confining stiffness of the hydrogel was varied by about two orders of magnitude. Yet, interestingly it was observed that the growth rate of the biofilms is constant with time (and inferred spatially uniform) and independent of the confining stiffness even though the swelling process was not. These results are shown in Figure 11. The time evolution of the growth volume ratio from multiple experiments is overlaid in Figure 11(a) where it can be seen that the growth rate is constant. The swelling ratio reaches a steady value during growth and the steady value is plotted as function of the stiffness ratio of confinement to the biofilm in Figure 11(b), along with the growth rate. Note that from our earlier results in Section 5.2.1, we expect the growth rate to be suppressed by increasing stiffness of the confining medium. We will resolve this seeming contradiction in this section and demonstrate the ability of the theory to model the experimental results.

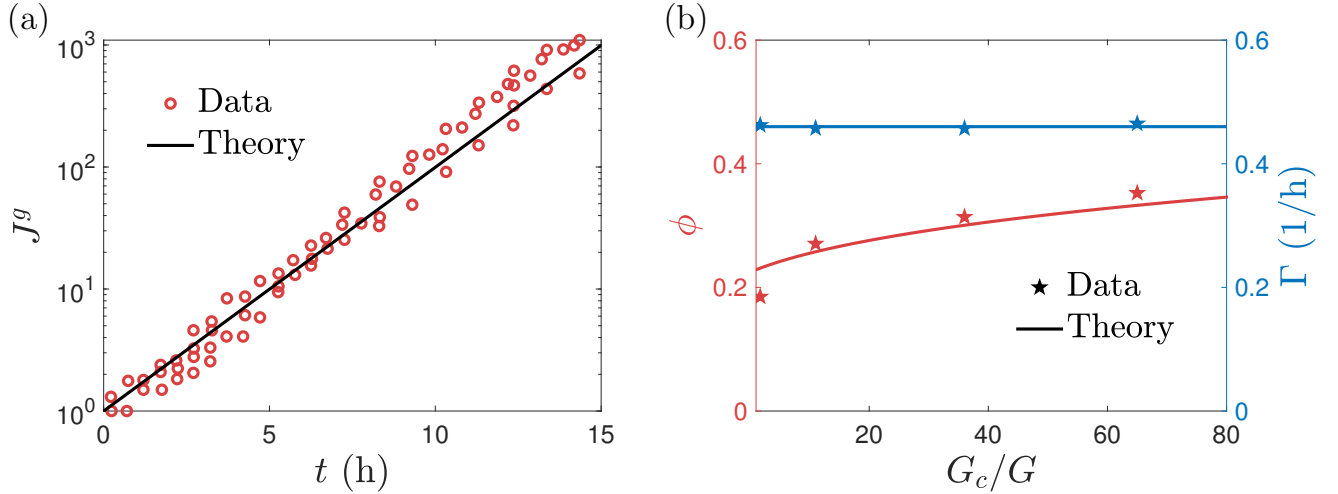


Figure 11: Comparison of experimental data (Zhang et al., 2021) and theoretical predictions for swelling-growth of bacterial biofilms. (a) Temporal evolution of the growth volume ratio. (b) The solid volume fraction (ϕ) and growth rate (Γ) as a function of ratio of shear modulus of confinement to shear modulus of biofilm (G_c/G).

In a previous study, we analysed the morphogenesis in these biofilms as they grow using an energy minimization approach (Li et al., 2022). However, we focused our attention to morphogenesis and used a kinematic prescription for the volumetric growth while neglecting swelling since it was shown experimentally that the growth rate remained constant and spatially uniform. Here instead, we will neglect the morphogenesis and use our swelling growth theory considering spherical geometry (so that we can use eq. (96) for the pressure applied by confining medium) to capture the swelling dependence and explain the growth rate behaviour. We first note that since the initial size ($R_0 = L_*$) is small ($\sim 1 \mu\text{m}$), the diffusion timescale is small compared to the growth timescale ($\tau_g/\tau_d \sim 1 \times 10^5$ for typical $D \sim 10^{-7} \text{ cm}^2/\text{s}$) and we can comfortably employ the infinitely fast diffusion approximation. Since the confinement is a thick medium, we set $B/A \rightarrow \infty$ (and thus $\lambda_b \rightarrow 1$) in eq. (97). Further, since the swelling reaches a steady value during growth, the pressure applied by the confinement must saturate for large deformations. Thus, we assume a neo-Hookean free energy function for the confining medium ($n = 0$ in eq. (95)) such that the applied pressure P_b in eq. (96) saturates at a cavitation pressure¹¹ value of $2.5G_c$. Further, the growth rate being independent of the confining stiffness, is possible if the homeostatic pressure of the system is very high compared to the maximum confining stiffness such that $P_h \gg \max(G_c)$. If this is the case, since $P_b \sim G_c$, the pressure ratio $P_b/P_h \rightarrow 0$ irrespective of the confining stiffness varying by two orders of magnitude. From the dependence of volumetric growth rate on P_b/P_h in Figure 5(d), it can be inferred that the dimensionless growth rate will be approximately unity irrespective of the confinement if $P_b/P_h \rightarrow 0$. Since the maximum value of stiffness ratio G_c/G is ~ 100 , all we need to capture the growth rate independence is to require $\bar{P}_h \gg 100$.

With the above discussion in mind, we choose the material parameters in Table 2 to model the experiments using the swelling growth theory in the infinitely fast diffusion limit (Section 5.2).

¹¹While in reality the pressure might saturate from damage in the confinement, for our analysis here only the peak pressure is relevant for which the cavitation limit of neo-Hookean model is a good approximation

The steady value of swelling is obtained by setting $\bar{P}_b = 2.5G_c/G$ in eq. (90). Predictions of the swelling growth theory agree with the experimental data shown in Figure 11. We note that the difference from our results in Section 5.2.1 arises from two factors - (i) the confining medium is non-stiffening ($n = 0$) so that the applied pressure saturates and (ii) we have chosen $\eta = -10$ here, which corresponds to a highly favourable conversion energy in comparison to the choice of $\eta = 0.95$ previously. In principle, any value of $\Delta\mu_0$ greater than the value chosen in Table 2 will also produce the same results. Essentially, if the conversion energy is favourable enough, it maintains the growth rate irrespective of changes in swelling ratio due to mechanical confinement. Or equivalently, if the conversion energy is favourable enough, the homeostatic pressure will be high (see Figure 5(b)) compared to even the largest confining stiffness. We hypothesize that the underlying cellular mechanism that leads to this high growth favourability is the use of a bacterial strain that is locked in a high cyclic diguanylate level (Zhang et al., 2021; Beyhan and Yildiz, 2007) and therefore always producing biofilm matrix. The swelling ratio however is independent of the conversion energy $\Delta\mu_0$ and only depends on the applied pressure (eq. (90)), its dependence on G_c/G has been captured in Figure 11(b) by fitting for χ . Thus our swelling-growth theory is able to successfully model both tumor and bacterial biofilm swelling-growth. We conclude the manuscript with a summary in the next section.

Table 2: Material parameter values for modelling of bacterial biofilm growth experiments

Quantity	Value	Source/Comment
G	1kPa	Zhang et al. (2021)
T	300 K	Room temperature
τ_g	2.17 h	Fitted from constant growth rate
χ	0.59	Fitted from ϕ vs G_c/G
$\Delta\mu_0$	105.88 MPa	Corresponds to $\eta = -10$
ω^f	$1.66 \times 10^{-28} \text{ m}^3/\text{molecule}$	Hong et al. (2008)

6. Summary and conclusions

Biological systems exhibit a vast array of growth phenomena that inherently rely on the coupling between large deformations and diffusion of constituents that are needed to feed the growth. Existing models of growth typically employ experimentally motivated phenomenological prescriptions to capture the consequences of this coupling by prescribing the directionality of growth (i.e. anisotropy), its rate, and the conditions required for it to stop (i.e. a homeostatic stress and a critical concentration of diffusing species). In this work, we investigate the coupled nature of growth by development of a thermodynamically consistent and mass conserving large deformation swelling-growth theory. The theory considers a solid body permeated by a representative diffusing species whose conversion into additional solid material leads to growth while the remaining diffusing species swells the growing solid. The mechanics is modelled by treating the mixture as a single homogenized continuum body, which circumvents difficulties of mixture theory. The driving stress for growth is identified using the dissipation inequality, and a kinetic

growth law is prescribed. It is shown that this framework successfully captures experiments of growing tumors and bacterial biofilms under diverse diffusion-consumption and mechanical constraints without the conventionally employed phenomenological prescriptions.

Several insights are drawn from the theory. Non-dimensionalization of the equations reveals the key role of the ratio between the shear modulus of the growing material and the characteristic chemical potential (i.e. G/μ^*); when this ratio is small, which is typically the case for soft swelling and growing systems, our choice of growth laws here predict nearly isotropic growth unless large and highly non-spherical dimensionless stresses are reached. This explains why conventional growth studies that often employ the assumption of isotropic growth for these systems fare well. In the same limit of small G/μ^* , it is shown that the growth driving stress is primarily a function of the species conversion energy per unit volume and the swelling ratio (i.e. $\Delta\mu_0$ and J_s) and the existence of a critical swelling ratio that stops growth is established. It is shown that the critical swelling ratio simultaneously captures the effect of two conventionally imposed phenomenological prescriptions - (i) a critical concentration of diffusing species that stops growth and (ii) a homeostatic pressure that the system tends to and stops growing at for uniform pressure loading in absence of diffusion-consumption constraints. Through the latter, the theory offers a kinetic basis for the homeostatic stress in relation to underlying material parameters, and explains why it is typically observed to be compressive for soft growing systems driven by swelling. Nonetheless, it is shown that for a general boundary value problem, the kinetic growth law does not specify a fixed stress-state that stops growth, thus emphasizing the potential pitfalls of phenomenological prescriptions, as experimental observations under specific conditions need not translate to other scenarios. Further, the kinetic growth law based on the driving stress is also able to qualitatively explain experimentally observed dependence of growth on concentration of diffusing species, namely the increase in growth rate with concentration, and saturation of growth rate at high concentration values. A critical conversion energy below which growth is never possible irrespective of the swelling is also established.

The ability of the theory to account for large deformations in both swelling and growth, in contrast to several studies in the literature, opens up a new avenue for investigation of the spontaneous emergence of nonlinear morphological growth phenomena such as growth induced wrinkling, buckling, fracture, and cavitation, which have been conventionally studied via inverse methods using kinematic assumptions. However, the theory is not without limitations, for example, directional growth mechanisms are not accounted for and need to be introduced to obtain anisotropic homeostatic stress-states. Also, the model cannot account for specific cellular biological processes involved in growth which are homogenized as an effective species conversion. The conversion energy $\Delta\mu_0$, though physically motivated must be determined experimentally; its estimation from homogenization of experimental data for cellular processes is non-trivial, future work could potentially embed biological models in service of such estimation. To describe the growth process in greater detail like in several mixture growth theories, such as by accounting for micro-environment, multiplicity of cell species, and inter diffusion of multiple components including nutrients, growth factors, and drugs, the theory needs to be generalized to account for multiple reaction-diffusion equations. Finally, the primary physics predicted by the theory has been established in this manuscript by solving boundary value problems with simple geometry. Future work should consider more complex geometries to study morphogenesis under mechanical

constraints and breakage of symmetry.

References

- Abi-Akl, R., Abeyaratne, R., Cohen, T., 2019. Kinetics of surface growth with coupled diffusion and the emergence of a universal growth path. *Proceedings of the Royal Society A* 475 (2221), 20180465.
- Afshar, A., Di Leo, C. V., 2021. A thermodynamically consistent gradient theory for diffusion–reaction–deformation in solids: Application to conversion-type electrodes. *Journal of the Mechanics and Physics of Solids* 151, 104368.
- Alessandri, K., Sarangi, B. R., Gurchenkov, V. V., Sinha, B., Kießling, T. R., Fetler, L., Rico, F., Scheuring, S., Lamaze, C., Simon, A., et al., 2013. Cellular capsules as a tool for multicellular spheroid production and for investigating the mechanics of tumor progression in vitro. *Proceedings of the National Academy of Sciences* 110 (37), 14843–14848.
- Amar, M. B., Chatelain, C., Ciarletta, P., 2011. Contour instabilities in early tumor growth models. *Physical review letters* 106 (14), 148101.
- Ambrosi, D., Ateshian, G. A., Arruda, E. M., Cowin, S., Dumais, J., Goriely, A., Holzapfel, G. A., Humphrey, J. D., Kemkemer, R., Kuhl, E., et al., 2011. Perspectives on biological growth and remodeling. *Journal of the Mechanics and Physics of Solids* 59 (4), 863–883.
- Ambrosi, D., Guana, F., 2007. Stress-modulated growth. *Mathematics and mechanics of solids* 12 (3), 319–342.
- Ambrosi, D., Guillou, A., 2007. Growth and dissipation in biological tissues. *Continuum Mechanics and Thermodynamics* 19 (5), 245–251.
- Ambrosi, D., Mollica, F., 2002. On the mechanics of a growing tumor. *International journal of engineering science* 40 (12), 1297–1316.
- Ambrosi, D., Mollica, F., 2004. The role of stress in the growth of a multicell spheroid. *Journal of mathematical biology* 48 (5), 477–499.
- Ambrosi, D., Preziosi, L., 2002. On the closure of mass balance models for tumor growth. *Mathematical Models and Methods in Applied Sciences* 12 (05), 737–754.
- Ambrosi, D., Preziosi, L., Vitale, G., 2010. The insight of mixtures theory for growth and remodeling. *Zeitschrift für angewandte Mathematik und Physik* 61 (1), 177–191.
- Anand, L., 2023. Introduction to Coupled Theories in Solid Mechanics. Unpublished MIT 2.077 course notes.
- Araujo, R. P., McElwain, D. S., 2004. A history of the study of solid tumour growth: the contribution of mathematical modelling. *Bulletin of mathematical biology* 66 (5), 1039–1091.
- Ateshian, G. A., 2007. On the theory of reactive mixtures for modeling biological growth. *Biomechanics and modeling in mechanobiology* 6 (6), 423–445.

- Ateshian, G. A., Morrison III, B., Holmes, J. W., Hung, C. T., 2012. Mechanics of cell growth. *Mechanics research communications* 42, 118–125.
- Ateshian, G. A., Nims, R. J., Maas, S., Weiss, J. A., 2014. Computational modeling of chemical reactions and interstitial growth and remodeling involving charged solutes and solid-bound molecules. *Biomechanics and modeling in mechanobiology* 13, 1105–1120.
- Ateshian, G. A., Ricken, T., 2010. Multigenerational interstitial growth of biological tissues. *Biomechanics and modeling in mechanobiology* 9, 689–702.
- Azeloglu, E. U., Albro, M. B., Thimmappa, V. A., Ateshian, G. A., Costa, K. D., 2008. Heterogeneous transmural proteoglycan distribution provides a mechanism for regulating residual stresses in the aorta. *American Journal of Physiology-Heart and Circulatory Physiology* 294 (3), H1197–H1205.
- Baek, S., Srinivasa, A., 2004. Diffusion of a fluid through an elastic solid undergoing large deformation. *International Journal of non-linear Mechanics* 39 (2), 201–218.
- Bertuzzi, A., Fasano, A., Gandolfi, A., Sinisgalli, C., 2010. Necrotic core in emt6/ro tumour spheroids: Is it caused by an atp deficit? *Journal of theoretical biology* 262 (1), 142–150.
- Beyhan, S., Yildiz, F. H., 2007. Smooth to rugose phase variation in vibrio cholerae can be mediated by a single nucleotide change that targets c-di-gmp signalling pathway. *Molecular microbiology* 63 (4), 995–1007.
- Biot, M. A., 1941. General theory of three-dimensional consolidation. *Journal of applied physics* 12 (2), 155–164.
- Biot, M. A., Temple, G., 1972. Theory of finite deformations of porous solids. *Indiana University Mathematics Journal* 21 (7), 597–620.
- Bistri, D., Di Leo, C. V., 2023. A continuum electro-chemo-mechanical gradient theory coupled with damage: Application to li-metal filament growth in all-solid-state batteries. *Journal of the Mechanics and Physics of Solids* 174, 105252.
- Bouklas, N., Huang, R., 2012. Swelling kinetics of polymer gels: comparison of linear and non-linear theories. *Soft Matter* 8 (31), 8194–8203.
- Boulinger, P., Hayes, M., 2001. Finite-amplitude waves in Mooney-Rivlin and Hadamard materials. Springer.
- Bryers, J. D., 2008. Medical biofilms. *Biotechnology and bioengineering* 100 (1), 1–18.
- Byrne, H. M., King, J. R., McElwain, D. S., Preziosi, L., 2003. A two-phase model of solid tumour growth. *Applied Mathematics Letters* 16 (4), 567–573.
- Carpio, A., Cebrián, E., Vidal, P., 2019. Biofilms as poroelastic materials. *International Journal of Non-Linear Mechanics* 109, 1–8.

- Casciari, J. J., Sotirchos, S. V., Sutherland, R. M., 1992. Variations in tumor cell growth rates and metabolism with oxygen concentration, glucose concentration, and extracellular ph. *Journal of cellular physiology* 151 (2), 386–394.
- Chalut, K. J., Janmey, P. A., 2014. Clamping down on tumor proliferation. *Biophysical journal* 107 (8), 1775.
- Chatelain, C., Balois, T., Ciarletta, P., Amar, M. B., 2011. Emergence of microstructural patterns in skin cancer: a phase separation analysis in a binary mixture. *New Journal of Physics* 13 (11), 115013.
- Chen, Z., 2018. From a thin membrane to an unbounded solid: dynamics and instabilities in radial motion of nonlinearly viscoelastic spheres. Ph.D. thesis, Massachusetts Institute of Technology.
- Chester, S. A., Anand, L., 2010. A coupled theory of fluid permeation and large deformations for elastomeric materials. *Journal of the Mechanics and Physics of Solids* 58 (11), 1879–1906.
- Chester, S. A., Anand, L., 2011. A thermo-mechanically coupled theory for fluid permeation in elastomeric materials: application to thermally responsive gels. *Journal of the Mechanics and Physics of Solids* 59 (10), 1978–2006.
- Ciarletta, P., Ambrosi, D., Maugin, G., Preziosi, L., 2013. Mechano-transduction in tumour growth modelling. *The European Physical Journal E* 36 (3), 1–9.
- Ciarletta, P., Foret, L., Ben Amar, M., 2011. The radial growth phase of malignant melanoma: multi-phase modelling, numerical simulations and linear stability analysis. *Journal of the Royal Society Interface* 8 (56), 345–368.
- Croix, B. S., Rak, J. W., Kapitain, S., Sheehan, C., Graham, C. H., Kerbel, R. S., 1996. Reversal by hyaluronidase of adhesion-dependent multicellular drug resistance in mammary carcinoma cells. *JNCI: Journal of the National Cancer Institute* 88 (18), 1285–1296.
- Curatolo, M., Gabriele, S., Teresi, L., 2017. Swelling and growth: a constitutive framework for active solids. *Meccanica* 52 (14), 3443–3456.
- Dervaux, J., Amar, M. B., 2011. Buckling condensation in constrained growth. *Journal of the Mechanics and Physics of Solids* 59 (3), 538–560.
- DiCarlo, A., Quiligotti, S., 2002. Growth and balance. *Mechanics Research Communications* 29 (6), 449–456.
- Doi, M., 2009. Gel dynamics. *Journal of the Physical Society of Japan* 78 (5), 052001.
- Duda, F. P., Souza, A. C., Fried, E., 2010. A theory for species migration in a finitely strained solid with application to polymer network swelling. *Journal of the Mechanics and Physics of Solids* 58 (4), 515–529.
- Faghihi, D., Feng, X., Lima, E. A., Oden, J. T., Yankeelov, T. E., 2020. A coupled mass transport and deformation theory of multi-constituent tumor growth. *Journal of the Mechanics and Physics of Solids* 139, 103936.

- Flory, P. J., 1942. Thermodynamics of high polymer solutions. *The Journal of chemical physics* 10 (1), 51–61.
- Fraldi, M., Carotenuto, A. R., 2018. Cells competition in tumor growth poroelasticity. *Journal of the Mechanics and Physics of Solids* 112, 345–367.
- Fung, Y.-c., 2013. *Biomechanics: motion, flow, stress, and growth*. Springer Science & Business Media.
- Garikipati, K., Arruda, E. M., Gosh, K., Narayanan, H., Calve, S., 2004. A continuum treatment of growth in biological tissue: the coupling of mass transport and mechanics. *Journal of the Mechanics and Physics of Solids* 52 (7), 1595–1625.
- Garteiser, P., Doblaz, S., Daire, J.-L., Wagner, M., Leitao, H., Vilgrain, V., Sinkus, R., Van Beers, B. E., 2012. Mr elastography of liver tumours: value of viscoelastic properties for tumour characterisation. *European radiology* 22, 2169–2177.
- Goriely, A., Moulton, D. E., Vandiver, R., 2010. Elastic cavitation, tube hollowing, and differential growth in plants and biological tissues. *Europhysics Letters* 91 (1), 18001.
- Greenspan, H., 1972. Models for the growth of a solid tumor by diffusion. *Studies in Applied Mathematics* 51 (4), 317–340.
- Helmlinger, G., Netti, P. A., Lichtenbeld, H. C., Melder, R. J., Jain, R. K., 1997. Solid stress inhibits the growth of multicellular tumor spheroids. *Nature biotechnology* 15 (8), 778–783.
- Hlatky, L., Sachs, R. K., Alpen, E. L., 1988. Joint oxygen-glucose deprivation as the cause of necrosis in a tumor analog. *Journal of cellular physiology* 134 (2), 167–178.
- Hong, W., Zhao, X., Zhou, J., Suo, Z., 2008. A theory of coupled diffusion and large deformation in polymeric gels. *Journal of the Mechanics and Physics of Solids* 56 (5), 1779–1793.
- Huggins, M. L., 1941. Solutions of long chain compounds. *The Journal of chemical physics* 9 (5), 440–440.
- Humphrey, J., Rajagopal, K., 2002. A constrained mixture model for growth and remodeling of soft tissues. *Mathematical models and methods in applied sciences* 12 (03), 407–430.
- Jain, R. K., 2005. Normalization of tumor vasculature: an emerging concept in antiangiogenic therapy. *Science* 307 (5706), 58–62.
- Jain, R. K., Martin, J. D., Stylianopoulos, T., 2014. The role of mechanical forces in tumor growth and therapy. *Annual review of biomedical engineering* 16, 321–346.
- Kerbel, R., Rak, J., Kobayashi, H., Man, M., Croix, B. S., Graham, C., 1994. Multicellular resistance: a new paradigm to explain aspects of acquired drug resistance of solid tumors. In: *Cold Spring Harbor symposia on quantitative biology*. Vol. 59. Cold Spring Harbor Laboratory Press, pp. 661–672.

- Kim, Y., Stolarska, M. A., Othmer, H. G., 2011. The role of the microenvironment in tumor growth and invasion. *Progress in biophysics and molecular biology* 106 (2), 353–379.
- Kobayashi, H., Man, S., Graham, C. H., Kapitain, S. J., Teicher, B. A., Kerbel, R. S., 1993. Acquired multicellular-mediated resistance to alkylating agents in cancer. *Proceedings of the National Academy of Sciences* 90 (8), 3294–3298.
- Koike, C., McKee, T., Pluen, A., Ramanujan, S., Burton, K., Munn, L., Boucher, Y., Jain, R., 2002. Solid stress facilitates spheroid formation: potential involvement of hyaluronan. *British journal of cancer* 86 (6), 947–953.
- Konica, S., Sain, T., 2020. A thermodynamically consistent chemo-mechanically coupled large deformation model for polymer oxidation. *Journal of the Mechanics and Physics of Solids* 137, 103858.
- Köpf, M. H., Pismen, L. M., 2013. A continuum model of epithelial spreading. *Soft matter* 9 (14), 3727–3734.
- Kuhl, E., 2014. Growing matter: a review of growth in living systems. *Journal of the Mechanical Behavior of Biomedical Materials* 29, 529–543.
- Levitas, V. I., Attariani, H., 2014. Anisotropic compositional expansion in elastoplastic materials and corresponding chemical potential: Large-strain formulation and application to amorphous lithiated silicon. *Journal of the Mechanics and Physics of Solids* 69, 84–111.
- Li, J., Kothari, M., Chockalingam, S., Henzel, T., Zhang, Q., Li, X., Yan, J., Cohen, T., 2022. Nonlinear inclusion theory with application to the growth and morphogenesis of a confined body. *Journal of the Mechanics and Physics of Solids* 159, 104709.
- Liu, Z., Toh, W., Ng, T. Y., 2015. Advances in mechanics of soft materials: A review of large deformation behavior of hydrogels. *International Journal of Applied Mechanics* 7 (05), 1530001.
- Loeffel, K., Anand, L., 2011. A chemo-thermo-mechanically coupled theory for elastic–viscoplastic deformation, diffusion, and volumetric swelling due to a chemical reaction. *International Journal of Plasticity* 27 (9), 1409–1431.
- Lubarda, V. A., Hoger, A., 2002. On the mechanics of solids with a growing mass. *International journal of solids and structures* 39 (18), 4627–4664.
- Lucantonio, A., Nardinocchi, P., Teresi, L., 2013. Transient analysis of swelling-induced large deformations in polymer gels. *Journal of the Mechanics and Physics of Solids* 61 (1), 205–218.
- Mattei, M., Frunzo, L., D’acunto, B., Pechaud, Y., Pirozzi, F., Esposito, G., 2018. Continuum and discrete approach in modeling biofilm development and structure: a review. *Journal of mathematical biology* 76 (4), 945–1003.
- McMahon, J., Goriely, A., Tabor, M., 2010. Spontaneous cavitation in growing elastic membranes. *Mathematics and mechanics of solids* 15 (1), 57–77.

- Menzel, A., Kuhl, E., 2012. Frontiers in growth and remodeling. *Mechanics research communications* 42, 1–14.
- Monod, J., 1949. The growth of bacterial cultures. *Annual review of microbiology* 3 (1), 371–394.
- Mooney, M., 1940. A theory of large elastic deformation. *Journal of applied physics* 11 (9), 582–592.
- Mpekris, F., Angeli, S., Pirentis, A. P., Stylianopoulos, T., 2015. Stress-mediated progression of solid tumors: effect of mechanical stress on tissue oxygenation, cancer cell proliferation, and drug delivery. *Biomechanics and modeling in mechanobiology* 14 (6), 1391–1402.
- Myers, K., Ateshian, G. A., 2014. Interstitial growth and remodeling of biological tissues: tissue composition as state variables. *Journal of the mechanical behavior of biomedical materials* 29, 544–556.
- Nadell, C. D., Drescher, K., Wingreen, N. S., Bassler, B. L., 2015. Extracellular matrix structure governs invasion resistance in bacterial biofilms. *The ISME journal* 9 (8), 1700–1709.
- Narayanan, H., Arruda, E., Grosh, K., Garikipati, K., 2009. The micromechanics of fluid–solid interactions during growth in porous soft biological tissue. *Biomechanics and modeling in mechanobiology* 8, 167–181.
- Narayanan, H., Verner, S., Mills, K., Kemkemer, R., Garikipati, K., 2010. In silico estimates of the free energy rates in growing tumor spheroids. *Journal of Physics: Condensed Matter* 22 (19), 194122.
- Oden, J. T., Lima, E. A., Almeida, R. C., Feng, Y., Rylander, M. N., Fuentes, D., Faghihi, D., Rahman, M. M., DeWitt, M., Gadde, M., et al., 2016. Toward predictive multiscale modeling of vascular tumor growth. *Archives of Computational Methods in Engineering* 23 (4), 735–779.
- Olive, P. L., Durand, R. E., 1994. Drug and radiation resistance in spheroids: cell contact and kinetics. *Cancer and Metastasis Reviews* 13 (2), 121–138.
- Preziosi, L., 2003. *Cancer modelling and simulation*. CRC Press.
- Rivlin, R. S., 1948. Large elastic deformations of isotropic materials iv. further developments of the general theory. *Philosophical transactions of the royal society of London. Series A, Mathematical and physical sciences* 241 (835), 379–397.
- Rodriguez, E. K., Hoger, A., McCulloch, A. D., 1994. Stress-dependent finite growth in soft elastic tissues. *Journal of biomechanics* 27 (4), 455–467.
- Roose, T., Netti, P. A., Munn, L. L., Boucher, Y., Jain, R. K., 2003. Solid stress generated by spheroid growth estimated using a linear poroelasticity model. *Microvascular research* 66 (3), 204–212.
- Sacco, R., Causin, P., Lelli, C., Raimondi, M. T., 2017. A poroelastic mixture model of mechanobiological processes in biomass growth: theory and application to tissue engineering. *Meccanica* 52 (14), 3273–3297.

- Salvadori, A., McMeeking, R., Grazioli, D., Magri, M., 2018. A coupled model of transport-reaction-mechanics with trapping. part i—small strain analysis. *Journal of the Mechanics and Physics of Solids* 114, 1–30.
- Sarntinoranont, M., Rooney, F., Ferrari, M., 2003. Interstitial stress and fluid pressure within a growing tumor. *Annals of biomedical engineering* 31, 327–335.
- Seminara, A., Angelini, T. E., Wilking, J. N., Vlamakis, H., Ebrahim, S., Kolter, R., Weitz, D. A., Brenner, M. P., 2012. Osmotic spreading of bacillus subtilis biofilms driven by an extracellular matrix. *Proceedings of the National Academy of Sciences* 109 (4), 1116–1121.
- Stylianopoulos, T., Martin, J. D., Chauhan, V. P., Jain, S. R., Diop-Frimpong, B., Bardeesy, N., Smith, B. L., Ferrone, C. R., Hornicek, F. J., Boucher, Y., et al., 2012. Causes, consequences, and remedies for growth-induced solid stress in murine and human tumors. *Proceedings of the National Academy of Sciences* 109 (38), 15101–15108.
- Taber, L. A., 1998. A Model for Aortic Growth Based on Fluid Shear and Fiber Stresses. *Journal of Biomechanical Engineering* 120 (3), 348–354.
- Thorne, R. G., Hrabetová, S., Nicholson, C., 2004. Diffusion of epidermal growth factor in rat brain extracellular space measured by integrative optical imaging. *Journal of neurophysiology* 92 (6), 3471–3481.
- Treloar, L. G., 1975. *The physics of rubber elasticity*. OUP Oxford.
- Ward, J. P., King, J. R., 1997. Mathematical modelling of avascular-tumour growth. *Mathematical Medicine and Biology: A Journal of the IMA* 14 (1), 39–69.
- Xue, S.-L., Li, B., Feng, X.-Q., Gao, H., 2016. Biochemomechanical poroelastic theory of avascular tumor growth. *Journal of the Mechanics and Physics of Solids* 94, 409–432.
- Xue, S.-L., Yin, S.-F., Li, B., Feng, X.-Q., 2018. Biochemomechanical modeling of vascular collapse in growing tumors. *Journal of the Mechanics and Physics of Solids* 121, 463–479.
- Yan, J., Nadell, C. D., Stone, H. A., Wingreen, N. S., Bassler, B. L., 2017. Extracellular-matrix-mediated osmotic pressure drives vibrio cholerae biofilm expansion and cheater exclusion. *Nature communications* 8 (1), 1–11.
- Zhang, Q., Li, J., Nijjer, J., Lu, H., Kothari, M., Alert, R., Cohen, T., Yan, J., 2021. Morphogenesis and cell ordering in confined bacterial biofilms. *Proceedings of the National Academy of Sciences* 118 (31), e2107107118.

Acknowledgements

The authors acknowledge our collaborators at Yale University, and in particular Professor Jing Yan, whose experiments motivated this study. We would also like to acknowledge Professor Lallit Anand for drawing attention to some useful references. Additionally, we thank Joseph Bonavia and Hudson Borja da Rocha for feedback on the manuscript. Finally we thank the reviewers who were helpful in bringing greater clarity to the mass balance and entropy inequality.

Appendix A. Theory

Appendix A.1. Mass balance during growth

Consider the current mass density of the solid matrix, ρ , whose evolution is given by the equation

$$\frac{\partial \rho}{\partial t} + \operatorname{div}(\rho \mathbf{v}) = \dot{\rho} + \rho \operatorname{div} \mathbf{v} = \tilde{\rho} \quad (\text{A.1})$$

where $\tilde{\rho}$ is the mass density supply rate to the solid matrix from the diffusing species and $v = \dot{\mathbf{x}}$ is the velocity of the material point. Based on standard kinematics of a continuum, it is known that $\dot{J} = J \operatorname{div} \mathbf{v}$, whose substitution into the mass balance equation above produces

$$\dot{\rho}_R = \tilde{\rho}_R, \quad (\text{A.2})$$

where $\rho_R = \rho J$ is the current solid mass per unit dry reference volume and $\tilde{\rho}_R = \tilde{\rho} J$ is the referential mass density supply rate to the solid matrix (mass supplied per unit dry reference volume per unit time). Thus ρ_R only changes during growth ($\tilde{\rho}_R \neq 0$). Since we assumed that the density of the solid matrix remains constant (at value ρ_0^m) during the growth process through the mapping by \mathbf{F}^g , we can write $\rho_R = \rho_0^m J^g$, the substitution of which in eq. (A.2) yields

$$\rho_0^m \dot{J}^g = \tilde{\rho}_R \quad (\text{A.3})$$

Recognizing $\rho_0^m \equiv 1/\Omega^m$ and $\tilde{\rho}_R \equiv \dot{\xi}_R$, we see that eq. (A.3) is equivalent to eq. (15).

Appendix A.2. Dissipation inequality

Under isothermal conditions, the entropy inequality can be written as

$$\int_{\mathbf{P}} \dot{\eta}_R \, dV_R \geq \int_{\partial \mathbf{P}} \mu_\eta (-\mathbf{j}_R \cdot \mathbf{n}_R) \, dA_R \quad (\text{A.4})$$

where η_R is the entropy per unit dry reference volume of the fluid-solid continuum within the dry material region \mathbf{P} and μ_η is the entropy supply per unit reference volume of the diffusing species, into \mathbf{P} through the boundary. Neglecting kinetic energy (or inertial effects) and assuming no body forces, the balance law for energy under isothermal conditions can be written as

$$\int_{\mathbf{P}} \dot{\epsilon}_R \, dV_R = \int_{\partial \mathbf{P}} (\mathbf{S} \mathbf{n}_R) \cdot \dot{\boldsymbol{\varphi}} \, dA_R + \int_{\partial \mathbf{P}} \mu_\epsilon (-\mathbf{j}_R \cdot \mathbf{n}_R) \, dA_R \quad (\text{A.5})$$

where ϵ_R is the internal energy per unit dry reference volume of the fluid-solid continuum within the dry material region \mathbf{P} and μ_ϵ is the internal energy supply per unit dry reference volume of the diffusing species, into \mathbf{P} through the boundary. Introducing the Helmholtz free energy per unit dry reference volume of the fluid-solid continuum, $\psi_R = \epsilon_R - \theta \eta_R$, where θ is the constant absolute temperature, we can write the following rate relation under isothermal conditions

$$\dot{\psi}_R = \dot{\epsilon}_R - \theta \dot{\eta}_R \quad (\text{A.6})$$

Defining the chemical potential μ as follows (see also Salvadori et al. (2018); Anand (2023)),

$$\mu = \mu_\epsilon - \theta \mu_\eta \quad (\text{A.7})$$

eqs. (A.4), (A.5), and (A.6) can be combined to write the dissipation inequality in eq. (21). Next, we show the localization of eq. (21) into eq. (22). We rewrite the first term on the right hand side of eq. (21) as follows

$$\int_{\partial P} (\mathbf{S}\mathbf{n}_R) \cdot \dot{\boldsymbol{\varphi}} \, dA_R = \int_{\partial P} \left(\mathbf{S} \cdot \frac{\partial \dot{\boldsymbol{\varphi}}}{\partial \mathbf{X}} + (\text{Div } \mathbf{S}) \cdot \dot{\boldsymbol{\varphi}} \right) dV_R = \int_{\partial P} \mathbf{S} \cdot \dot{\mathbf{F}} \, dV_R \quad (\text{A.8})$$

where we have employed the divergence theorem, the mechanical equilibrium equation (20), and the definition of \mathbf{F} in eq. (1). Next, consider the second term on the right hand side of eq. (21),

$$\int_{\partial P} \mu(-\mathbf{j}_R \cdot \mathbf{n}_R) \, dA_R = \int_{\partial P} (-\mathbf{j}_R \cdot \nabla \mu - \mu \text{Div } \mathbf{j}_R) \, dV_R = \int_{\partial P} \left(-\mathbf{j}_R \cdot \nabla \mu + \mu (J^g j^s + J^s j^g) \right) dV_R \quad (\text{A.9})$$

where we have used the divergence theorem and the isochoric diffusion-consumption equation (18). Plugging eqs. (A.8) and (A.9) into eq. (21) and localizing the integral gives the required inequality in eq. (22) (see also Loeffel and Anand (2011); Levitas and Attariani (2014); Konica and Sain (2020); Afshar and Di Leo (2021); Bistri and Di Leo (2023)).

Appendix A.3. Stress power

We prove the stress power equivalence stated in eq. (23) below. First, using eqs. (7), (8) and (20), we write

$$\mathbf{S} \cdot \dot{\mathbf{F}} = (\mathbf{S}\mathbf{F}^T) \cdot \mathbf{L} = J\mathbf{T} \cdot \mathbf{L} = J\mathbf{T} \cdot \left(\mathbf{L}^e + \mathbf{F}^e \mathbf{L}^g \mathbf{F}^{e-1} + \frac{j^s}{3J^s} \mathbf{I} \right) \quad (\text{A.10})$$

We now consider the first term in eq. (A.10),

$$J\mathbf{T} \cdot \mathbf{L}^e = J\mathbf{T} \cdot (\dot{\mathbf{F}}^e \mathbf{F}^{e-1}) = (J\mathbf{T}\mathbf{F}^{e-T}) \cdot \dot{\mathbf{F}}^e = J^s J^g (J^e \mathbf{T}\mathbf{F}^{e-T}) \cdot (\mathbf{F}^{e-T} \mathbf{F}^{eT} \dot{\mathbf{F}}^e) \quad (\text{A.11})$$

$$= J^s J^g (J^e \mathbf{F}^{e-1} \mathbf{T}\mathbf{F}^{e-T}) \cdot (\mathbf{F}^{eT} \dot{\mathbf{F}}^e) = J^s J^g \mathbf{T}^e \cdot \text{sym}(\mathbf{F}^{eT} \dot{\mathbf{F}}^e) = \frac{1}{2} J^s J^g \mathbf{T}^e \cdot \dot{\mathbf{C}}^e \quad (\text{A.12})$$

where we have used eqs. (3) and (8), the definition of \mathbf{T}^e in eq. (24)₂ and its symmetry¹². Next, we consider the second term in eq. (A.10),

$$J\mathbf{T} \cdot (\mathbf{F}^e \mathbf{L}^g \mathbf{F}^{e-1}) = (J\mathbf{F}^{eT} \mathbf{T}\mathbf{F}^{e-T}) \cdot \mathbf{L}^g = J^g (J^{es} \mathbf{F}^{esT} \mathbf{T}\mathbf{F}^{es-T}) \cdot \mathbf{L}^g = J^g \mathbf{M}^{es} \cdot \mathbf{L}^g \quad (\text{A.13})$$

where we have used eqs. (1) and (3), and the definition of \mathbf{M}^{es} in eq. (24)₁. Finally, we consider the third term in eq. (A.10),

$$J\mathbf{T} \cdot \left(\frac{j^s}{3J^s} \mathbf{I} \right) = \frac{Jj^s}{3J^s} \text{tr}(\mathbf{T}) \quad (\text{A.14})$$

Using eqs. (A.11)–(A.14) in eq. (A.10) gives us the desired relation in eq. (23).

¹² \mathbf{Z} is symmetric if $\mathbf{Z} = \text{sym}(\mathbf{Z})$ where $\text{sym}(\mathbf{Z}) = \frac{1}{2}(\mathbf{Z} + \mathbf{Z}^T)$. If \mathbf{Z} is symmetric, $\mathbf{Z} \cdot \mathbf{Y} = \mathbf{Z} \cdot \text{sym}(\mathbf{Y})$.

Appendix A.4. Non-isochoric conversion reaction

In this section, we generalize the theory to non-isochoric species conversion ($\Omega^f \neq \Omega^m$). Following the same derivation procedure in the manuscript while using the non-isochoric diffusion-consumption equation (17) instead of the isochoric version in eq. (18) gives us the desired theory. Skipping the straightforward math, we present here directly the key equations that will differ for the non-isochoric version of the theory from the equations for the isochoric case in the manuscript. The only extra parameter that shows up in the theory is the ratio $\alpha = \Omega^f/\Omega^m = \rho_0^m/\rho_0^f$ which is the referential density ratio of the solid to diffusing species. The growth driving stress \mathbf{T}^g in eq. (34) is now instead

$$\mathbf{T}^g = \mathbf{M}^{es} + \left(\Delta\mu_0^{\text{nis}} + (J^s + \alpha - 1) \left(\frac{\partial\psi_g}{\partial J^s} - \frac{1}{3} J^e \text{tr}(\mathbf{T}) \right) - \psi_g \right) \mathbf{I} \quad (\text{A.15})$$

where $\Delta\mu_0^{\text{nis}} = \Delta\mu_0 + \mu_0^f(\alpha - 1)$ is the chemical conversion energy per unit referential solid volume for conversion of unit mass of diffusing species to solid. The driving stress for volumetric growth in eq. (41)₂ is now instead

$$f_g = (\alpha - 1) \left(\frac{\partial\psi_g}{\partial J^s} - \frac{1}{3} J^e \text{tr}(\mathbf{T}) \right) + \Delta\mu_0^{\text{nis}} + J^s \frac{\partial\psi_g}{\partial J^s} - \psi_g \quad (\text{A.16})$$

$$= (\alpha - 1) (\mu - \mu_0^f) + \Delta\mu_0^{\text{nis}} + J^s \frac{\partial\psi_g}{\partial J^s} - \psi_g \quad (\text{A.17})$$

where the chemical potential μ from eq. (32)₂ remains unchanged along with the growth evolution equations (63),(66). The specialized form of f_g for the chosen constitutive functions in Section 3 is given by

$$f_g = \Delta\mu_0^{\text{nis}} + (\alpha - 1) (\mu^{\text{mix}}(\phi) - K \ln(J^e)\phi) + f_g^{\text{mix}}(\phi) + f_g^{\text{mech}} \quad (\text{A.18})$$

where expressions for $\mu^{\text{mix}}(\phi)$, f_g^{mix} , and f_g^{mech} can be found in eqs. (61), (64) and (65).

For the boundary value problem in Section 5.2 where we consider the limit of infinitely fast diffusion, we have $\mu = \mu_0^f$ and thus f_g in eq. (A.17) reduces to

$$f_g = \Delta\mu_0^{\text{nis}} + J^s \frac{\partial\psi_g}{\partial J^s} - \psi_g \quad (\text{A.19})$$

Thus it can be seen that the driving stress f_g in this case has essentially the same functional form as for the isochoric case in eq. (41)₂ except that $\Delta\mu_0$ has been replaced by $\Delta\mu_0^{\text{nis}}$. Thus all the conclusions devised for the isochoric case in Section 5.2 also hold for the non-isochoric case.

Appendix A.5. $\bar{\Gamma}$ dependence on η

Now we demonstrate that in the limit of small G/μ^* , a larger value of the conversion energy ratio η , when all other parameters are fixed, leads to a smaller dimensionless growth rate for a given $\phi > \phi^f$. In the limit of small G/μ^* , the dimensionless growth rate can be written using eqs. (75) and (83), for the choice of $\bar{f}_g^* = \bar{f}_g(\phi^f)$, as

$$\bar{\Gamma} = \frac{\Delta\bar{\mu}_0 + \bar{f}_g^{\text{mix}}(\phi)}{\Delta\bar{\mu}_0 + \bar{f}_g^{\text{mix}}(\phi^f)} = 1 + \frac{\bar{f}_g^{\text{mix}}(\phi) - \bar{f}_g^{\text{mix}}(\phi^f)}{\Delta\bar{\mu}_0 + \bar{f}_g^{\text{mix}}(\phi^f)} \quad (\text{A.20})$$

We first note from Sections 5.1 and 5.2 that ϕ^f and $\Delta\bar{\mu}_0^c$ are independent of η when χ is fixed. Thus when all other parameters are fixed, a larger value of η corresponds to a smaller value of $\Delta\mu_0$, and for any given ϕ for which $\bar{f}_g^{\text{mix}}(\phi) < \bar{f}_g^{\text{mix}}(\phi^f)$, the dimensionless growth rate will be smaller for larger η using eq. (A.20). Hence, to demonstrate the claim at the start of the section, it only remains to show that \bar{f}_g^{mix} is a monotonically decreasing function of ϕ for $\phi > \phi^f$ such that $\phi > \phi^f$ necessitates $\bar{f}_g^{\text{mix}}(\phi) < \bar{f}_g^{\text{mix}}(\phi^f)$. In Section 5.1, it was established that \bar{f}_g^{mix} is always monotonically decreasing with ϕ for $\chi \leq 0.5$. Defining $\phi_{\text{max}} = 1/J_{\text{max}}^s$, where J_{max}^s was defined in Section 5.1 as the swelling ratio at which \bar{f}_g attains its maximum value, we note that \bar{f}_g^{mix} is a monotonically decreasing function of ϕ for $\phi > \phi_{\text{max}}$. For $\chi > 0.5$, we numerically verified that $\phi_f > \phi_{\text{max}}$ in the limit $G/\mu^* \rightarrow 0$. Thus \bar{f}_g^{mix} is always a monotonically decreasing function of ϕ for $\phi > \phi^f$, irrespective of the value of χ , and hence the claim at the start of the section holds true.

Appendix B. Perfectly incompressible limit

Here we consider the perfectly incompressible limit of the theory so that $K/G \rightarrow \infty$ and $J^e \rightarrow 1$. In rate form this means that $\dot{J}^e = J^e \text{tr}(\dot{\mathbf{F}}^e \mathbf{F}^{e-1}) = \mathbf{F}^{e-T} \cdot \dot{\mathbf{F}}^e = 0$. We do the following manipulation to rewrite this constraint

$$\begin{aligned} \mathbf{F}^{e-T} \cdot \dot{\mathbf{F}}^e &= \mathbf{F}^{e-T} \cdot \left(\mathbf{F}^{e-T} \mathbf{F}^{eT} \dot{\mathbf{F}}^e \right) = \left(\mathbf{F}^{e-1} \mathbf{F}^{e-T} \right) \cdot \left(\mathbf{F}^{eT} \dot{\mathbf{F}}^e \right) \\ &= \mathbf{C}^{e-1} \cdot \left(\mathbf{F}^{eT} \dot{\mathbf{F}}^e \right) = \mathbf{C}^{e-1} \cdot \text{sym} \left(\mathbf{F}^{eT} \dot{\mathbf{F}}^e \right) = \mathbf{C}^{e-1} \cdot \dot{\mathbf{C}}^e = 0 \end{aligned} \quad (\text{B.1})$$

where we have used the definition of \mathbf{C}^e in eq. (6) and its symmetry. We can thus add an arbitrary scalar times $\mathbf{C}^{e-1} \cdot \dot{\mathbf{C}}^e$ to the stress power in eq. (23),

$$\mathbf{S} \cdot \dot{\mathbf{F}} = \frac{1}{2} J^s J^g \mathbf{T}^e \cdot \dot{\mathbf{C}}^e + J^g \mathbf{M}^{es} \cdot \mathbf{L}^g + \frac{J J^s}{3 J^s} \text{tr}(\mathbf{T}) + \frac{1}{2} J^g (P \mathbf{C}^{e-1}) \cdot \dot{\mathbf{C}}^e \quad (\text{B.2})$$

where P is an arbitrary scalar field (the Lagrange multiplier associated with the incompressibility constraint). Following the same process in the manuscript, we can now show that

$$\mathbf{T} = \frac{1}{J^s} \left(2 \mathbf{F}^e \frac{\partial \psi_g}{\partial \mathbf{C}^e} \mathbf{F}^{eT} - P \mathbf{I} \right), \quad \mathbf{M}^{es} = J^s \mathbf{F}^{esT} \mathbf{T} \mathbf{F}^{es-T}, \quad \mathbf{T}^e = \mathbf{F}^{e-1} \mathbf{T} \mathbf{F}^{e-T} \quad (\text{B.3})$$

while the Piola stress is given by (20)₃. All other quantities and prescriptions in Section 3 apart from the above stresses remain unchanged.

The specific form the mechanical free energy in eq. (57) now reads

$$\hat{\psi}_g^{\text{mech}}(\mathbf{C}^e, J^s) = \frac{G}{2} \left((J^s)^{\frac{2}{3}} \text{tr}(\mathbf{C}^e) - 3 - 2 \ln(J^s) \right) \quad (\text{B.4})$$

The modified expressions in Section 4 for the incompressible limit are written below¹³ (unchanged

¹³A quick way to obtain the incompressible equations from the compressible theory is to set $K \ln(J^e) \rightarrow (G-P)$.

expressions are not listed again for brevity),

$$\mathbf{T} = \frac{1}{J^s} (G\mathbf{B}^{es} - P\mathbf{I}), \quad \mathbf{M}^{es} = G\mathbf{C}^{es} - P\mathbf{I} \quad (\text{B.5})$$

$$\mu = \mu_0^f + \mu^* (\ln(1 - \phi) + \phi + \chi\phi^2) - G\phi + P\phi \quad (\text{B.6})$$

$$f_g^{\text{mech}} = G \left(\ln(J^s) - \frac{1}{6} (\text{tr}(\mathbf{C}^{es}) - 3) \right) \quad (\text{B.7})$$

For the case of non-isochoric species conversion, the total driving stress f_g for volumetric growth is given by

$$f_g = \Delta\mu_0^{\text{mis}} + f_g^{\text{mix}} + f_g^{\text{mech}} + (\alpha - 1) (\mu^{\text{mix}}(\phi) - G\phi + P\phi) \quad (\text{B.8})$$

where f_g^{mech} in the incompressible limit is expressed in eq. (B.7).

Appendix B.1. Uniform spherical fields in limit of infinitely fast diffusion

Consider the uniform swelling-growth problem in Section 5.2 where we assume infinitely fast diffusion, now with the added constraint of perfect incompressibility. The uniform elastic deformation field is now $\mathbf{F}^e = \mathbf{I}$ since $J^e = 1$. Using this along with eq. (87)_{4,5} in eqs. (B.5) and (B.6), we arrive at the following equations

$$-P_b = \phi \left(G\phi^{-\frac{2}{3}} - P \right), \quad \mu^{\text{mix}}(\phi) - G\phi + P\phi = 0 \quad (\text{B.9})$$

Eliminating P from the two equations and non dimensionalising the resulting equation yields eq. (90). Further, substituting $\mathbf{F}^e = \mathbf{I}$ in eq. (B.7) results in the following equation

$$f_g^{\text{mech}} = G \left(\ln(J^s) - \frac{1}{2} \left((J^s)^{\frac{2}{3}} - 1 \right) \right) \quad (\text{B.10})$$

so that the driving force is purely a function of the swelling ratio or solid volume fraction for the uniform swelling-growth problem in the infinitely fast diffusion limit with perfect incompressibility,

$$f_g = f_g^\infty = \Delta\mu_0^{\text{mis}} + f_g^{\text{mix}}(\phi) + G \left(\ln(\phi^{-1}) - \frac{1}{2} \left(\phi^{-\frac{2}{3}} - 1 \right) \right) \quad (\text{B.11})$$

In the case of isochoric species conversion, $\Delta\mu_0^{\text{mis}} = \Delta\mu_0$. Non-dimensionalizing the result yields eq. (92).

Appendix C. Numerical implementation

Here we outline the numerical procedure used to solve the spherically symmetric governing equations in Section 5.3, which is written formally in Algorithm 1. The spatial domain \bar{R} was discretized using $N = 200$ equally spaced points. The mechanical and swelling equilibrium equations were solved using finite difference schemes that solve a nonlinear system of equations using Matlab's 'fsolve' solver while supplying the Jacobian matrix (derivative of residual with respect to the variables) using the 'SpecifyObjectiveGradient' option. An exact analytical expression for the Jacobian matrix was coded for the mechanical equilibrium solver while an approximate Jacobian matrix was supplied for the swelling equilibrium solver (which was sufficient for fast enough

convergence). Simultaneous mechanical and swelling equilibrium is ensured using a staggered scheme that is run till convergence. The evolution equations for growth were integrated using a fourth order Runge-Kutta (RK4) scheme. After a convergence analysis in time, a conservative value of $d\bar{t}_g \sim 10^{-3}$ was chosen for the stepping size of the time integration.

Appendix C.1. Confinement dimensions for tumor growth simulations

The dimensions of the confining shells used for simulating Cases B-D of the tumor growth experiments are listed in Table C.3 where the inner volume of the confinement is given by $\frac{4}{3}\pi A^3$. The capsule volumes have been obtained from the dashed lines of Fig. 2E in Alessandri et al. (2013), a slight correction has been made for Case D such that the confinement volume is chosen based on the volume at which the tumor growth rate starts deviating from the free growth curve. The estimation of dimensions of the confining shells in Alessandri et al. (2013) is approximate and is inconsistent with the capsule volumes. Thus we have chosen representative dimension ratios (B/A) based on their reported values for thick and thin capsules.

Algorithm 1 Spherically Symmetric Swelling Growth

procedure SWELLINGGROWTH

 $\bar{t}_g, \bar{\lambda}_r^g, \bar{J}^g \leftarrow 0, \bar{1}, \bar{1}$
while $\bar{t}_g < \bar{t}_g^f$ **do**
 $\bar{\lambda}_r^g, \bar{J}^g \leftarrow \text{GROWTHSTEP}(\bar{\lambda}_r^g, \bar{J}^g, d\bar{t}_g)$
 $\bar{r}, \bar{J}^s \leftarrow \text{MECHSWELLEQB}(\bar{\lambda}_r^g, \bar{J}^g)$
 $\bar{t}_g \leftarrow \bar{t}_g + d\bar{t}_g$
end while
end procedure
procedure MECHSWELLEQB($\bar{\lambda}_r^g, \bar{J}^g$)

 $\bar{r} \leftarrow \text{MECHEQB}(\bar{J}^s, \bar{\lambda}_r^g, \bar{J}^g)$
do
 $\bar{J}^s \leftarrow \text{SWELLEQB}(\bar{r}, \bar{\lambda}_r^g, \bar{J}^g)$
 $\bar{\mu}_1 \leftarrow \text{CHEMPOT}(\bar{\lambda}_r^g, \bar{J}^g, \bar{r}, \bar{J}^s)$
 $\bar{r} \leftarrow \text{MECHEQB}(\bar{J}^s, \bar{\lambda}_r^g, \bar{J}^g)$
 $\bar{\mu}_2 \leftarrow \text{CHEMPOT}(\bar{\lambda}_r^g, \bar{J}^g, \bar{r}, \bar{J}^s)$
while $\|\bar{\mu}_2 - \bar{\mu}_1\| < \epsilon$
return \bar{r}, \bar{J}^s
end procedure
 \triangleright Staggered solver for equilibrium

 \triangleright Finite difference scheme that solves (104),(109)₁
 \triangleright Finite difference scheme that solves (105),(109)₂
 \triangleright Calculate $\bar{\mu}$ using (71)

 $\triangleright \epsilon$ is a small parameter to check convergence

procedure GROWTHSTEP($\bar{\lambda}_r^g, \bar{J}^g, d\bar{t}_g$)

 $\bar{y} \leftarrow [\bar{\lambda}_r^g, \bar{J}^g]$
 $\bar{k}_1 \leftarrow \text{DYDT}(\bar{y})$
 $\bar{k}_2 \leftarrow \text{DYDT}(\bar{y} + \frac{1}{2}\bar{k}_1 d\bar{t}_g)$
 $\bar{k}_3 \leftarrow \text{DYDT}(\bar{y} + \frac{1}{2}\bar{k}_2 d\bar{t}_g)$
 $\bar{k}_4 \leftarrow \text{DYDT}(\bar{y} + \bar{k}_3 d\bar{t}_g)$
 $\bar{y} \leftarrow \bar{y} + d\bar{t}_g/6 (\bar{k}_1 + 2\bar{k}_2 + 2\bar{k}_3 + \bar{k}_4)$
 $\bar{\lambda}_r^g, \bar{J}^g \leftarrow \bar{y}(1 : N), \bar{y}(N + 1, 2 : N)$
return $\bar{\lambda}_r^g, \bar{J}^g$
end procedure
 \triangleright RK4 integration scheme

 \triangleright Spatial domain \bar{R} is discretized using N points

procedure DYDT(\bar{y})

 $\bar{\lambda}_r^g, \bar{J}^g \leftarrow \bar{y}(1 : N), \bar{y}(N + 1 : 2N)$
 $\bar{r}, \bar{J}^s \leftarrow \text{MECHSWELLEQB}(\bar{\lambda}_r^g, \bar{J}^g)$
 $\bar{z}_1 \leftarrow \text{DLAMRGDT}(\bar{\lambda}_r^g, \bar{J}^g, \bar{r}, \bar{J}^s)$
 $\bar{z}_2 \leftarrow \text{DJGDT}(\bar{\lambda}_r^g, \bar{J}^g, \bar{r}, \bar{J}^s)$
return $[\bar{z}_1, \bar{z}_2]$
end procedure
 \triangleright Calculates $\frac{d\lambda_r^g}{dt_g}$ using (107)₁
 \triangleright Calculates $\frac{dJ^g}{dt_g}$ using (74)₄ and (75)

Table C.3: Dimensions of confinement in tumor growth experiments

Case	Inner Volume (mm ³)	B/A	J_c/\bar{J}_0
B	0.12	1.25	40
C	0.003	1.25	1
D	0.0034	1.12	1.135